

g12 Analysis Procedures, Statistics and Systematics

R.A. Badui C. Bookwalter S. Chandavar P. Eugenio J.T. Goetz
L. Guo K. Hicks V. Kubarovskiy M.C. Kunkel M. Paolone
W. Phelps J.W. Price M. Saini C. Salgado D. Schott
D.P. Weygand

December 1, 2014

Contents

1	Summary of Running Conditions	3
1.1	Trigger Configurations	3
1.2	Lists of Runs	7
2	Calibration and Detector Performance	11
2.1	Trigger Efficiency	11
2.2	Photon Tagger Calibration and Beam Energy Corrections	12
2.3	Start Counter Calibration and Resolution	22
2.3.1	Start Counter Efficiency	28
2.4	Drift Chamber Calibration and Resolution	29
2.4.1	Drift Chamber and TOF smearing parameters in gpp	29
2.4.2	Drift Chamber Wire Efficiency	30
2.5	Cerenkov Calibration and Resolution	30
2.5.1	Cerenkov Efficiency	30
2.6	Time-of-Flight Counter Calibration and Resolution	30
2.6.1	Time-of-Flight Counter Efficiency and Bad Paddles	30
2.6.2	ADC and TDC Values	31
2.7	Electrocalorimeter Calibration and Resolution	38
2.7.1	Electrocalorimeter Efficiency and Bad Paddles	38
3	Procedure for Data Analysis	38
3.1	“Pass1” Cooking and Data Reconstruction	38
3.2	Obtaining Reconstructed Data	39
3.3	g12-Specific Corrections	40
3.3.1	Final-State Particle Momentum Corrections	40
3.4	General Features of Lepton Data in g12	42
3.4.1	CC Comparison	43

3.4.2	EC Comparison	45
4	Flux Determination	53
4.1	Beam Trips	54
4.2	Normalized Yields for Different Beam Conditions	54
4.3	Run-by-run Stability and Systematic Uncertainty of Flux	54
5	Simulations	54
5.1	Generating Events for Digitization	54
5.2	Digitization and Smearing	55
5.3	Reconstruction of Simulated Data	61
5.4	Fiducial Region Selection	61
6	Other Systematics	65
6.1	Comparison of Data to Known Resonances	65
6.2	Comparison of Data to Known Cross Sections	65
References		66

Abstract

This document serves to summarize all information needed to process and analyze data from the CLAS *g12* experiment taken in the summer of 2008. This was a high-luminosity, high-energy real-photon run with a 65 nA circularly polarized beam, 40 cm unpolarized ℓH_2 target and an E_{beam} up to 5.7 GeV. The associated proposals, and therefore the trigger, focused on the high-energy part of the tagger, and though it was not part of the original proposals, the Cherenkov was active for most of the run.

1 Summary of Running Conditions

The *g12* experiment was a high-luminosity, high-energy real-photon run for CLAS. The electron beam current was 60–65 nA on the 40 cm ℓH_2 target. A total of 26×10^8 triggers were recorded using several of the 12 available trigger bits. The “production trigger” required two prongs (start-counter and time-of-flight coincidence) in two different sectors and in coincidence with a tagger hit at or above 3.6 GeV. There was secondary trigger which required three prongs, again in different sectors, regardless of tagger hits. The running conditions are summarized in Table 1. In addition to this document, there is a wealth of information to be found in the wiki pages at

<http://clasweb.jlab.org/rungroups/g12/wiki>

which has served as a repository for all things related to the *g12* experiment. The dissertations associated with this experiment contain a lot of information as well: dissertation

- John T. Goetz. “ Ξ Hyperon Photoproduction from Threshold to 5.4 GeV with the CEBAF Large Acceptance Spectrometer”. PhD thesis. University of California Los Angeles, 2010
- Craig Bookwalter. “A Search for Exotic Mesons in $\gamma p \rightarrow \pi^+ \pi^+ \pi^- n$ with CLAS at Jefferson Lab”. PhD thesis. Florida State University, 2012
- Diane Schott. “A Search for an Exotic Meson in the $\gamma p \rightarrow \Delta^{++} \pi^- \eta$ Reaction”. PhD thesis. Florida International University, 2012
- Mukesh Saini. “Search for New and Unusual Stangonia using CLAS”. PhD thesis. Florida State University, 2013
- Jason Bono. “First Time Measurements of Polarization Observables for the Charged Cascade Hyperon in Photoproduction”. PhD thesis. Florida International University, 2014

1.1 Trigger Configurations

The *g12* experiment was the first Hall *B* run-period to implement field programmable gate array (FPGA) processors to handle the trigger logic of the **ABBRCLAS** detector (see Sec. ??). With this new FPGA-powered triggering system, came the ability to modify the trigger quickly during the experiment. While potentially dangerous — these changes must be accounted for in total-cross-sectional analyses for example — this allowed the group to tune the trigger to get the highest possible rate of physical events.

The trigger bits used during the *g12* running period are defined in Tables 2, 3 and 4. They generally consisted of a number of tracks which were the coincidence of any one of the four start counter paddles and

Table 1: The running conditions of the *g12* experiment.

E_{beam} of photon	5.715 GeV
Beam Polarization	Circular
e^- Current	60–65 nA
Tagger Range	5% - 95% of e^- energy
Tagger Trigger Range	3.6–5.441 GeV
Torus Magnet	$\frac{1}{2}B_{\text{max}}$ (1930 A)
Target Length	40 cm
Target Center (z location)	-90 cm
Target Material	ℓH_2
Target Polarization	None
Start Counter Offset	0 cm
Radiator Thickness	10^{-4} radiation lengths
Collimator Radius	6.4 mm

any of the 57 time-of-flight paddles in a given sector as discussed in Sec. ???. The hardware and configuration did not allow triggering on two tracks in the same sector because there were only six signals coming from the TOF — one for each sector. The coincidence of these tracks with the photon tagger, called the “Master-OR,” is defined in Table 5.

There were two sets of thresholds for the EC labeled *photon* and *electron*. These labels did not mean photon or electron specifically, but were considered a first-order approximation. The actual particle identification was done much later in the analysis of the reconstructed data. The thresholds for the CC and EC during the *g12* running period are shown in Table 6.

Table 2: Trigger configuration for $g12$ runs from 56363 to 56594 and 56608 to 56647. $(ST \times TOF)_i$ indicates a single *prong* which is a trigger-level track defined as a coincidence between a start counter and time-of-flight hit in the i^{th} sector or any sector if the subscript index, i , is not specified. An added $\times 2$ or $\times 3$ indicates the coincidence of multiple *prongs* which are not in the same sector. MORA and MORB represent coincidences with tagger hits within a certain energy range as specified in Table 5.

$g12$ runs 56363–56594, 56608–56647			
bit	definition	L2 multiplicity	prescale
1	MORA·($ST \times TOF$) ₁ ·($ST \times TOF$)	–	1
2	MORA·($ST \times TOF$) ₂ ·($ST \times TOF$)	–	1
3	MORA·($ST \times TOF$) ₃ ·($ST \times TOF$)	–	1
4	MORA·($ST \times TOF$) ₄ ·($ST \times TOF$)	–	1
5	MORA·($ST \times TOF$) ₅ ·($ST \times TOF$)	–	1
6	MORA·($ST \times TOF$) ₆ ·($ST \times TOF$)	–	1
7	ST×TOF	–	1
8	MORA·($ST \times TOF$) $\times 2$	–	1
11 ^a	MORB·($ST \times TOF$) $\times 2$	–	1
12	($ST \times TOF$) $\times 3$	–	1

^abit 11 and MORB were included in the trigger starting with run 56519.

Table 3: Trigger configuration for $g12$ runs from 56595 to 56607 and 56648 to 57323. (EC×CC) represents a coincidence between the electromagnetic calorimeter and the Čerenkov subsystems within a single sector using the thresholds as described in Table 6. ECP represents the *photon* threshold trigger from the EC as detailed in Fig. ???. See Table 2 for other explanatory details.

$g12$ runs 56595–56607, 56648–57323			
bit	definition	L2 multiplicity ^a	prescale
1	MORA·($ST \times TOF$)	1	1000/300 ^b
2	MORA·($ST \times TOF$) $\times 2$	2/ ^c	1
3	MORB·($ST \times TOF$) $\times 2$	2	1
4	ST×TOF	1	1000/300
5	($ST \times TOF$)·ECP $\times 2$	1	1
6	($ST \times TOF$)·(EC×CC)	2	1
7	MORA·($ST \times TOF$)·(EC×CC)	–	1
8	MORA·($ST \times TOF$) $\times 2$	–	1
11	(EC×CC) $\times 2$	–	1
12	($ST \times TOF$) $\times 3$	–	1

^aLevel 2 triggering was turned off on all bits for runs 56605, 56607 and 56647.

^bPrescaling for bits 1 and 4 were 1000 for runs prior to 56668 at which point they both were changed to 300.

^cLevel 2 triggering of bit 2 was set to 2 for runs prior to 56665 at which point it was turned off.

Table 4: Trigger configuration for the single-sector runs of *g12*. Trigger bits 7–12 were not used for these runs. See Table 2 for explanatory details.

bit	definition	L2 multiplicity	prescale
1	MORA·(ST×TOF) ₁	sector 1	1
2	MORA·(ST×TOF) ₂	sector 2	1
3	MORA·(ST×TOF) ₃	sector 3	1
4	MORA·(ST×TOF) ₄	sector 4	1
5	MORA·(ST×TOF) ₅	sector 5	1
6	MORA·(ST×TOF) ₆	sector 6	1

Table 5: Master-OR definitions for *g12*. The TDC counters were used in the trigger and since each of these corresponds to several energy paddles, the energies given here are approximate. *T*-counter number 1 corresponds to the highest energy photon of approximately 5.4 GeV. Both MORA and MORB are referenced in terms of the trigger logic in Tables 2, 3 and 4. The *single-sector* runs are listed in Table 8.

run range	MORA		MORB	
	<i>T</i> -counters	energy (GeV)	<i>T</i> -counters	energy (GeV)
56363–56400	1–47	1.7–5.4	–	–
56401–56518	1–25	3.6–5.4	–	–
56519–57323	1–19	4.4–5.4	20–25	3.6–4.4
<i>single-sector</i>	1–31	3.0–5.4	–	–

Table 6: Threshold values for the electromagnetic calorimeter (EC) and Čerenkov counter (CC) during the *g12* running period. EC thresholds are shown as *inner/total*, and CC thresholds are shown as *left/right*.

EC		CC
<i>photon</i>	<i>electron</i>	
50/100 mV	60/80 mV	20/20 mV
150/300 MeV	180/240 MeV	~0.4 photo-electrons

1.2 Lists of Runs

The runs for this experiment range from 56855 to 57317 inclusive. The runs that made it into Tables. 7 and 8 qualified upon success of reconstructing final-state hadrons using the cooking program's default particle identification in coordination with the hand-written notes by the shift takers. Other runs of note include those used specifically for calibration in Table 9 and normalization, zero-field and empty-target runs in Table 10.

Table 7: List of successfully reconstructed production runs and their beam currents in nA.

runs current (nA)	runs current (nA)	runs current (nA)
56363 20	56605 60	56900-56908 60
56365 30	56608-56612 60	56914-56919 60
56369 30	56614-56618 60	56921-56922 60
56384 5	56620-56628 60	56923 65
56386 20	56630-56636 60	56924 70
56401 50	56638-56644 60	56925 80
56403 70	56646 60	56926-56930 60
56404 60	56653-56656 60	56932 60
56405 50	56660-56661 60	56935-56940 60
56406 40	56665-56670 60	56948-56956 60
56408 80	56673-56675 60	56958 60
56410 90	56679-56681 60	56960-56975 60
56420-56422 5	56683 60	56977-56980 60
56435 5	56685-56696 60	56992-56994 60
56436 15	56700-56708 60	56996-57006 60
56441 35	56710-56724 60	57008-57017 60
56442 30	56726-56744 60	57021-57023 60
56443 20	56748-56750 60	57025-57027 60
56445-56450 60	56751-56768 65	57030-57032 60
56453-56459 60	56770-56772 65	57036-57039 60
56460-56462 70	56774-56778 65	57062-57069 60
56465 70	56780-56784 65	57071-57073 60
56467-56472 70	56787-56788 65	57075-57080 60
56478-56483 70	56791-56794 65	57095-57097 60
56485-56487 70	56798-56802 65	57100-57103 60
56489-56490 70	56805-56815 65	57106-57108 60
56499 70	56821-56827 65	57114-57128 60
56501 60	56831-56834 65	57130-57152 60
56503 57	56838-56839 65	57159-57168 60
56504 56	56841-56845 65	57170-57185 60
56505-56506 40	56849 65	57189-57229 60
56508-56510 60	56853-56862 65	57233-57236 60

continued on next page.

continued from previous page.

runs	runs	runs			
current (nA)	current (nA)	current (nA)			
56513-56517	60	56864	65	57249-57253	60
56519	60	56865-56866	60	57255-57258	60
56521-56542	60	56870	65	57260-57268	60
56545-56550	60	56874-56875	60	57270-57288	60
56555-56556	60	56877	60	57290-57291	60
56561-56564	60	56879	60	57293-57312	60
56573-56583	60	56897-56898	60	57317	60
56586-56593	60	56899	65		

Table 9: A list of the runs which were calibrated for the subsystems: tagger (TAG), start counter (ST), and time-of-flight (TOF). The calibrations were committed into the database for the range starting with the run shown and ending with the run just prior to the next listed run. A brief reason for calibration is given in the last column.

run	systems affected	reason
56363	TAG, ST, TOF	start of run
56503	ST	ST adjustment
56508	"	" "
56661	TAG, ST, TOF	trigger and ST changes
56663	"	" "
56665	"	" "
56666	"	" "
56670	TAG	vacuum problem in tagger fixed
56673	TAG, ST, TOF	trigger change
56732	"	RF related problems fixed by Accelerator group
56765	TAG	T20 left HV problem
56766	"	T20 left HV adjusted
56782	TAG, ST, TOF	changes in calibration database
56855	"	" "
56923	"	start of intensity studies
57094	"	changes in calibration database
57154	ST	adjusted ST ADC timing in gate

Table 8: A list of the single-sector runs using the trigger configuration described in Table 4.

run	current (nA)	run	current (nA)
56476	24	56910	35
56502	24	56911	30
56520	24	56912	25
56544	24	56913	24
56559	24	56933-4	24
56585	24	56981-3 ^a	24
56619	24	56985 ^a	15
56637	24	56986	15
56663-4	24	56989	24
56697	24	57028	24
56725	24	57061	24
56747	24	57094 ^b	24
56769	24	57129	24
56804	24	57155-6	24
56835	24	57237-8	24
56869	5		

^aNo Level-2 trigger was used for runs 56981-56985^bA shorter ST ADC gate was implemented starting with run 57094.

Table 10: List of special calibration runs done during the *g12* experiment.

run	current (nA)	description
56397	0.05	normalization
56475	10	zero-field
56511	0.05	normalization, tagger TDC-left
56512	0.05	normalization, tagger TDC-right
56584	0.05	normalization
56682	0.05	normalization
56790	0.05	normalization
56931	0.05	normalization
56947	0.05	normalization
57169	0.05	normalization
57239	24	empty-target, single-sector
57241	80	empty-target, production
57248	0.05	normalization

A script named “g12runs” was created to provide a list of the runs which were fully reconstructed without errors. It can also provide a lot of information about each run including the beam current, the number of good scalar intervals, and the run type such as production, calibration, or single-sector. The script resides in the *clasg12* user’s home directory here:

```
/home/clasg12/local/scripts/g12runs
```

and has an extensive help message with the “-h” as shown here:

```
>/home/clasg12/local/scripts/g12runs -h
Usage:      usage: g12runs [options]
```

example to get all good data runs:

```
g12runs -t prod -t single -x calib
```

to get all data runs (prod and single) that have been completely cooked, sorted and have complete flux information:

```
g12runs -t pass1 -t flux -i
```

Options:

-h, --help	show this help message and exit
-r RANGE, --range=RANGE	

```

range of runs to print out (inclusive from:to) To get
the six-digit run numbers, use this range:
557313:557316. Can also be a single run number.
default: 56363:557316

-c CURRENT, --current=CURRENT
    range of currents to print out (inclusive from:to).
    examples: 40:80, 20:35 default: 0:90

-t RUNTYPE, --run-type=RUNTYPE
    Type of runs to print out. can be any of the
    following, and may be specified more than once: prod
    single calib cc dc norm pass1 flux Note: calib
    includes all norm runs. Use prod, single and calib to
    get all runs. default: prod, single

-x EXCLUDE, --exclude-type=EXCLUDE
    excludes types from being printed out. may be
    specified more than once.

-i, --intersect
    require all run types specified with the -t option to
    be valid. Note: "g12runs -tprod -tsingle -i" will
    result in no output since prod and single run types
    are mutually exclusive. Typical usage is to get runs
    that have complete pass1 and flux data: "g12runs
    -tpass1 -tflux -i".

-e, --extra-info
    print extra information for each run.

-m, --max-ind
    print maximum index for each run printed.

-n, --nfiles
    print number of files for each run printed.

-s SET, --set=SET
    print runs which correspond to one (or all by default)
    of ten groups: 1 - 10. These groups represent
    approximately 10% of the whole run period.

-a, --scalar
    Print out the number of scalar intervals in the form:
    good/total.

-d, --dump
    Dump all info about all runs.

```

2 Calibration and Detector Performance

The calibration of the raw data was done through seven incomplete but representative passes labeled `pass0_v1` through `pass0_v7` though only the last three of these is still available via JLab's mass storage system (`mss`). All calibration constants were put into the `calib_user.RunIndexg12` run index with the exception of certain lepton-specific numbers as discussed in Sec. 3.4.

2.1 Trigger Efficiency

In the first few weeks of *g12*, during “commissioning,” an attempt to determine the efficiency of the two-track trigger (bit 8 in Tables 2 and 3) was made. The rate of this main production trigger rose quadratically with the beam current while the physical event rate increased linearly. The number of accidentals, which

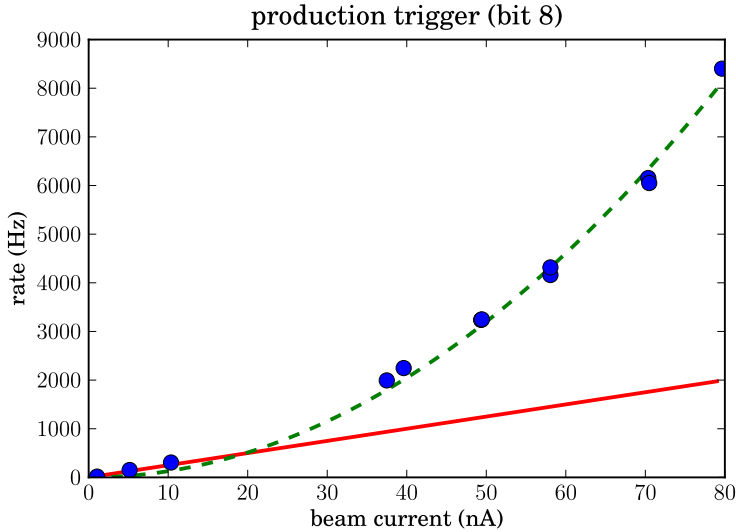


Figure 1: The production trigger rate (bit 8 in Tables 2 and 3) was measured for various beam currents shown by the blue dots. The rates below 10 nA are roughly linear and are extrapolated via the red solid line to show an estimate of the physical event rate. The actual trigger rate is fitted with a quadratic shown by the green dashed line. By this estimate, the accidental rate is shown to equal the physical event rate at approximately 40 nA. The *g12* experiment was done at 60–65 nA.

must be cut from any analysis, increased with increasing current and at a certain point, the majority of the events taken were accidentals. The trigger rate as a function of the beam current is shown in Fig. 1. An estimate of the linear part of the trigger rate shows that approximately 60% of the events recorded during the *g12* experiment (which ran at 60–65 nA beam current) were accidentals.

2.2 Photon Tagger Calibration and Beam Energy Corrections

The *g12* experiment had a complicated trigger which presented difficulties that were ironed out as described in this section. The problem was first noticed by *g12* participants at the analysis level in which missing particle masses were systematically low. It was realized while investigating the issue that the low missing particle mass was dependent on the run number and varied in mass as much as 10 MeV. There was also features in the run dependent missing mass that showed a constant low mass (run<56550) followed by a jump in mass which remained constant (56550<run<56920) until another jump in mass which seemed to produce a mass closer the PDG mass (run>56920). To analyze and correct for the cause of the problem, two topologies were chosen to isolate the missing particles, proton and neutron. The first topology;

$$\gamma p \rightarrow \pi^+ \pi^- [p] \quad (1)$$

was chosen to be the correction topology, while the second topology;

$$\gamma p \rightarrow \pi^+ \pi^+ \pi^- [n] \quad (2)$$

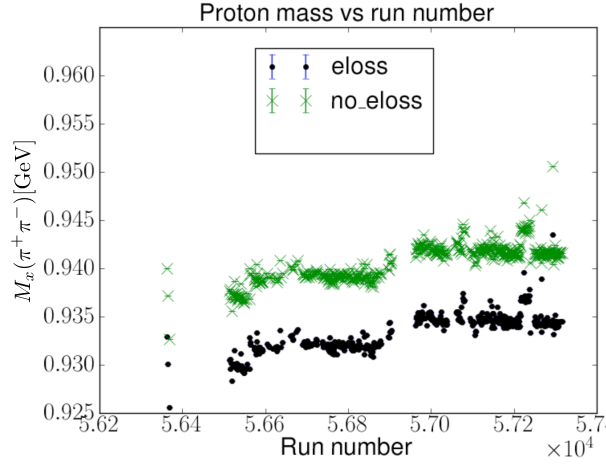


Figure 2: Plot of *g12* run number vs. proton mass with and without the “energy-loss” applied. PDG mass for the proton is 0.938272 GeV/c.

was chosen to verify the corrections obtained from eq. 1. The reasoning for choosing topology from eq. 1 as the correction topology is because all three particles can be detected, meaning inspecting the missing mass of $\pi^+\pi^-$, $M_x(\pi^+\pi^-)$, under the conditions of exclusivity should reveal the detected particle proton. This can be solved as follows using 4-vector notation;

$$(P_\gamma + P_{\text{target}} - (P_{\pi^+} + P_{\pi^-}))^2 = P_p = m_p^2 \quad (3)$$

where P_γ , P_{target} , P_{π^\pm} and P_p are the 4-vectors of the photon beam, target, π^\pm and proton respectively and m_p is the mass of the proton. The skim consisted of the data for the correction was of one CLAS PID π^+ , one CLAS PID π^- , one CLAS PID proton and nothing else. Exclusive cuts were then placed by requiring the missing energy, $M_E(p\pi^+\pi^-) < 0.025$ GeV and the missing mass squared of $M_x^2(p\pi^+\pi^-) < 0.015$ GeV². These cuts assure all events chosen exclude the topology;

$$\gamma p \rightarrow p \pi^+ \pi^- [\pi^0]$$

since the mass squared of $\pi^0 = 0.0182$ GeV².

The first step chosen was to verify whether the “energy-loss” correction was causing the discrepancy, this can be seen in Figs. 2, 3. It was concluded that the “energy-loss” correction was not the culprit of the problem. From Fig. 2, two runs were chosen, 56515 and 57130, in which the difference in the missing mass was ≈ 10 MeV. Inspecting the invariant mass, $M(\pi^+\pi^-)$, Fig 4, for runs 56515 and 57130 revealed only a mass deviation of ≈ 1.4 MeV in which disclosed that the problem with the *g12* data stream to be solely in the photon beam energy.

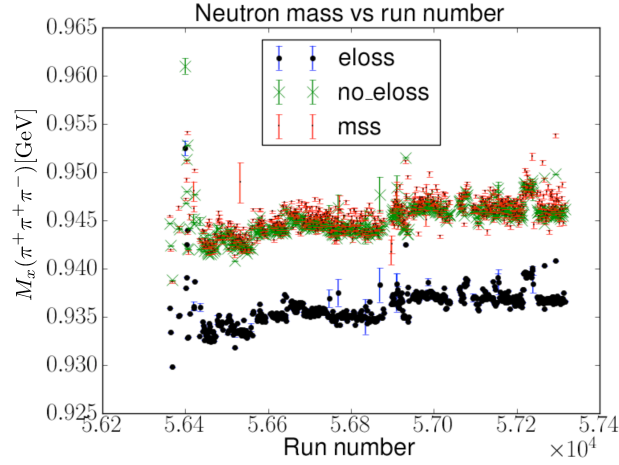


Figure 3: Plot of *g12* run number vs. neutron mass with and without the “energy-loss” applied. PDG mass for the neutron is 0.939565 GeV/c. Image Source: [bookwalter]

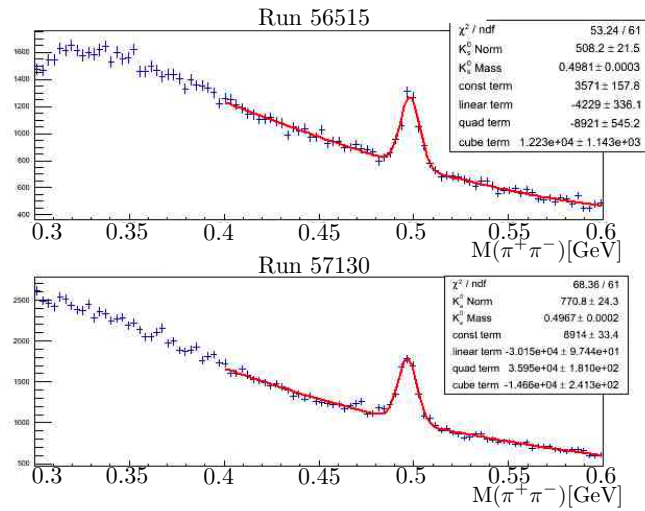


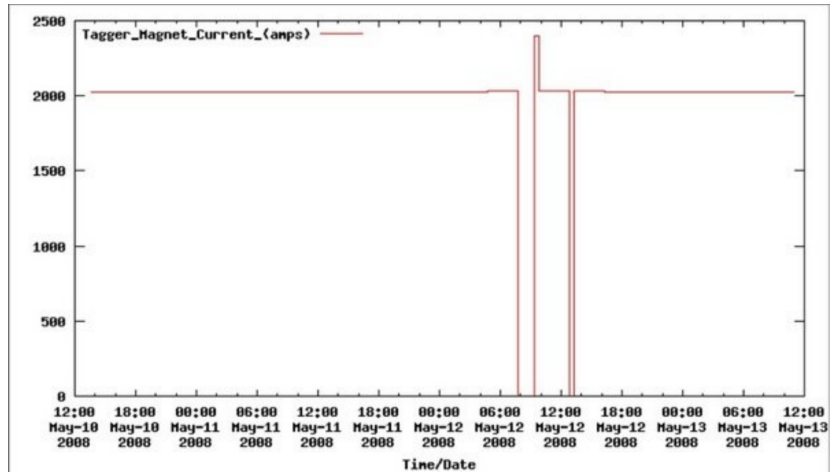
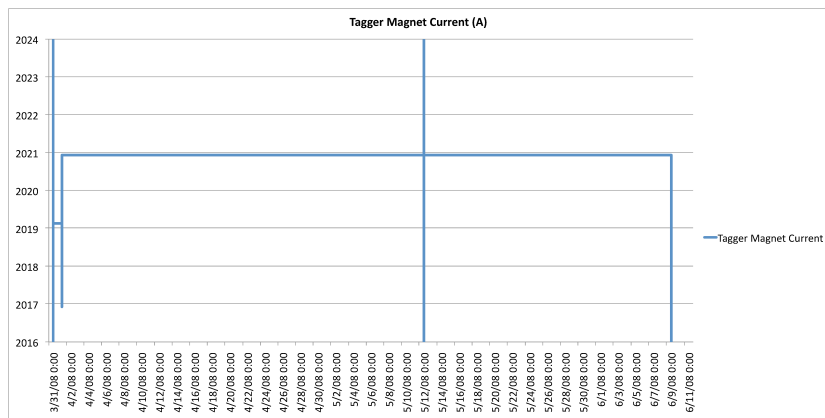
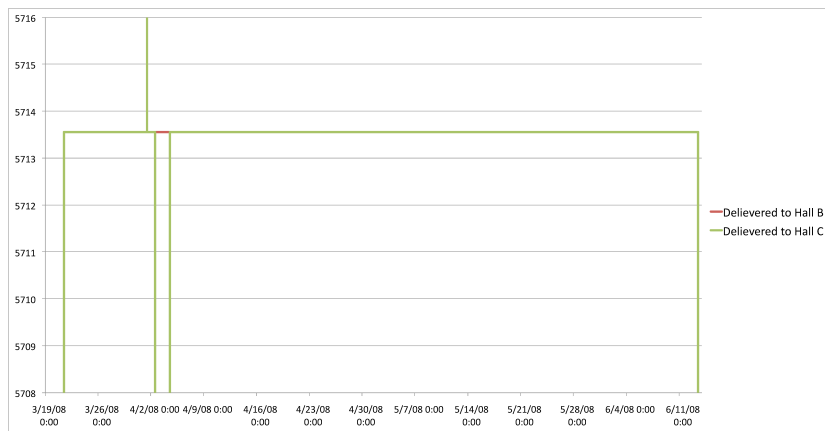
Figure 4: Plot of Kaon mass for runs 56515 and 57130. PDG mass for the kaon is 0.497614 GeV/c.

Now that it is known that the photon beam energy is the cause of the issue, it must be known the cause of the photon beam error. Several quantities that the tagger subsystem are subjected to were analyzed, first being the tagger magnet current which, according to the EPICS Fig 5, remain constant but showed that around run = 56920 (May 12, 2008) the tagger magnet was shut-off. The tagger magnet shut-off was done because work had to be done in the hall, however after the tagger magnet was turned on, the current was set to its previous setting. A further investigation into the tagger magnet was performed by private communication with the accelerator group chief Arne Freyberger, Fig 6 shows the data the accelerator group had for the tagger magnet which confirms that the tagger magnet current was stable throughout the running of g12. The next beam quantity analyzed was the beam current delivered by CEBAF, again through private communication with the accelerator group chief Arne Freyberger it is shown in Fig. 7 that the electron beam current remained constant throughout the g12 experiment.

The next quantity investigated was the positioning of the tagger dump. This quantity was used in place of the tagger magnetic field strength because hall b does not measure the tagger magnetic field strength, however since the radius of curvature a charged particle travels is proportional to the magnetic field, Eq. 4, this quantity is suitable.

$$p = q(v \times B)r \quad (4)$$

The y-positioning of the tagger dump jumps on or about May 12, 2008, Fig. 8. This would effect how the tagger recorded the scattered electron. A cause for the change in y-positioning can only be due to the magnetic field changing. The phenomena in magnetism that allows for a steady current but a change in magnetic field is known as hysteresis, Fig. 9 illustrates that on the x-axis there is a constant current that is associated with 2 distinct magnetic fields shown on the y-axis of Fig. 9.

**Figure 5:** Tagger magnet current according to EPICS**Figure 6:** Tagger magnet current according to accelerator group**Figure 7:** Electron beam current delivered to hall *b*(red) and hall *c* (green) according to accelerator group during the time of *g12* running

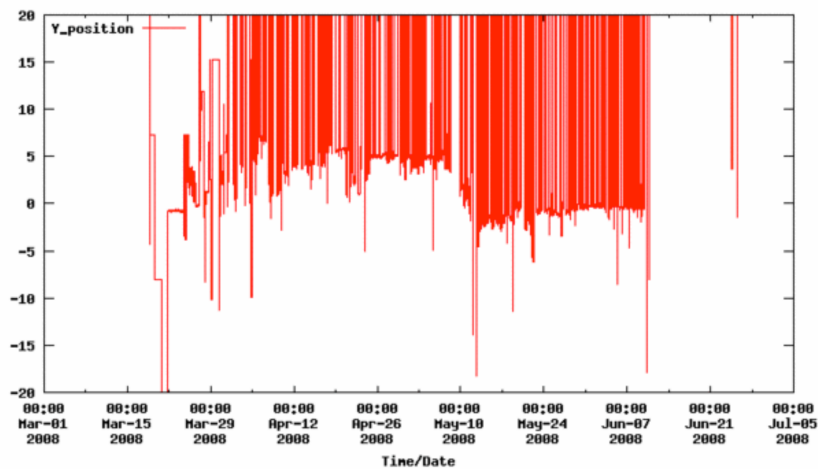


Figure 8: Tagger dump y-positioning according to EPICS

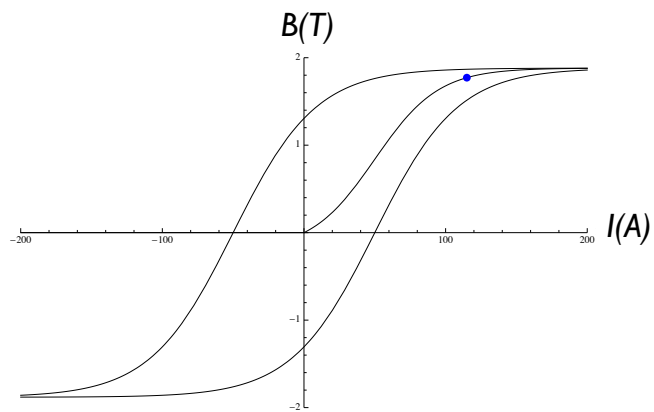


Figure 9: Plot depicting the process of hysteresis. For the a current of strength I , there could exist two magnetic fields of strength B .

Now that it is determined that the cause of the *g12* missing mass fluctuations are due to hysteresis and the effect would be on the scattered electron, the *g12* data stream was corrected in the following manner. Lets let

$$P_{\pi^+} + P_{\pi^-} = P_{\pi^+ \pi^-}$$

therefore

$$(P_\gamma + P_{\text{target}} - (P_{\pi^+ \pi^-}))^2 = m_p^2 \quad (5)$$

$$P_\gamma^2 + P_{\text{target}}^2 + P_{\pi^+ \pi^-}^2 + 2P_\gamma P_{\text{target}} - 2P_\gamma P_{\pi^+ \pi^-} - 2P_{\text{target}} P_{\pi^+ \pi^-} = m_p^2 \quad (6)$$

$$(7)$$

collecting terms of P_γ to one side and using $P_{\text{target}}^2 = m_p^2$ and $P_\gamma^2 = 0$

$$P_{\pi^+ \pi^-}^2 - 2P_{\text{target}} P_{\pi^+ \pi^-} = 2P_\gamma (P_{\pi^+ \pi^-} - P_{\text{target}}) \quad (8)$$

From this using eq. ?? in 4-vector notation

$$P_\gamma = P_{E_0} - P_e$$

where P_{E_0} is the beam energy delivered from CEBAF as recorded in the RUNC bank and P_e is the scattered electron in the *bremssstrahlung* process that is recorded by the tagger. From eq. ?? the only known quantities are P_{E_0} and P_γ . Applying a scalar correction to P_e as xP_e and solving for x for all known quantities, eq. 8 simplifies to;

$$x = \frac{P_{E_0}(P_{\text{target}} - P_{\pi^+ \pi^-}) + P_{\pi^+ \pi^-}^2/2 - P_{\text{target}} P_{\pi^+ \pi^-}}{(P_{E_0} - P_\gamma)(P_{\text{target}} - P_{\pi^+ \pi^-})} \quad (9)$$

To reduce statistical fluctuations $\frac{1}{10}$ of run 56515 was analyzed to obtain the correction factor x . The correction factor was fitted to a 3rd order polynomial ± 0.008 from the mean of the peak to establish an accurate measurement of the peak, this is shown in Fig 10. After the correction factor was extracted for run 56515, it was applied to both the topologies listed in Eq. 1 and Eq. 2 by recalculating the photon beam energy as;

$$\begin{aligned} E_e &= E_{\text{CEBAF}} - E_\gamma \\ E_\gamma^{new} &= E_{E_0} - E_e * x. \end{aligned}$$

Figures 11, 12 illustrate the missing mass topologies after beam correction and shows that the new calculated missing mass is less than 1 MeV from PDG values. Since both the missing proton mass and missing neutron mass were adjusted properly to the correct mass by using the same beam correction factor, it shows that the correction factor is independent of topology and therefore must be applied to all *g12* analyses. The procedure to calculate x was repeated for every run in *g12*, Fig 13, with $\frac{1}{10}$ of the data used. To validate the corrections of the entire *g12* data set, the missing neutron mass was recalculated for each run, shown in Fig. 14, using several correction schemes, i.e. a scheme of just “energy-loss” corrections, a scheme of “energy-loss” and momentum corrections (JTG PCor), a scheme of “energy-loss”, momentum corrections (JTG PCor) and beam corrections (MK BeamCor) and a scheme of “energy-loss” and beam corrections (MK BeamCor). It

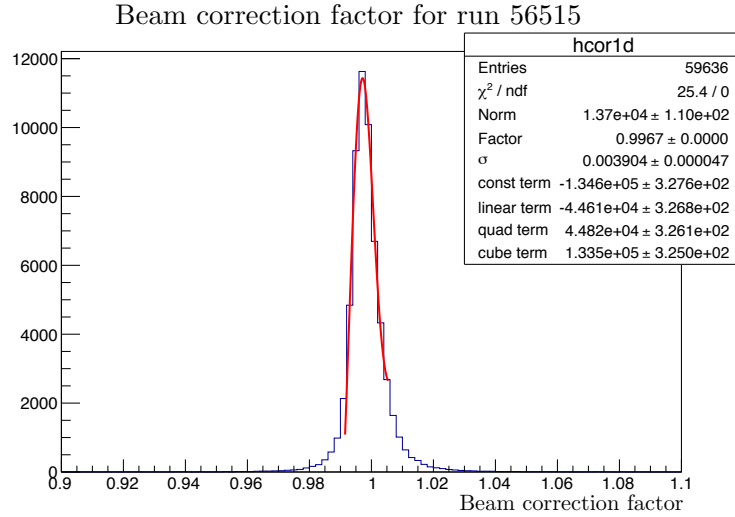


Figure 10: Beam correction factor for run 56515. The fit is a 3rd order polynomial ± 0.008 from the mean of the peak

can be seen in Fig. 14 that the only scheme that sufficed was the combination of “energy-loss” and beam corrections.

To correct for run by run shifts in the beam energy, use the header file in:

https://jlabsvn.jlab.org/svnroot/clas/trunk/analysis/g12/g12_ecor.hpp

In the analysis program, the user needs to have the run number of the event and the uncorrected beam energy, then use:

```
corrected_beam_energy(int run, double uncorrected_beam_energy)
```

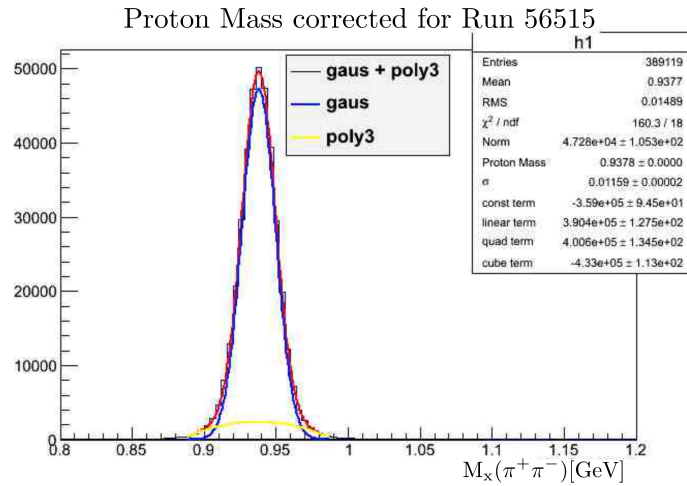


Figure 11: Plot of proton mass for runs 56515 after beam correction was applied. PDG mass for the proton is 0.938272 GeV/c.

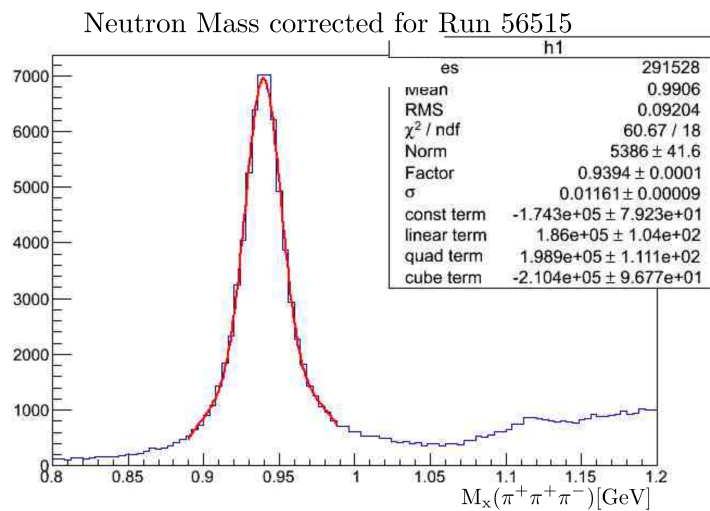


Figure 12: Plot of neutron mass for runs 56515 after beam correction was applied PDG mass for the neutron is 0.939565 GeV/c.

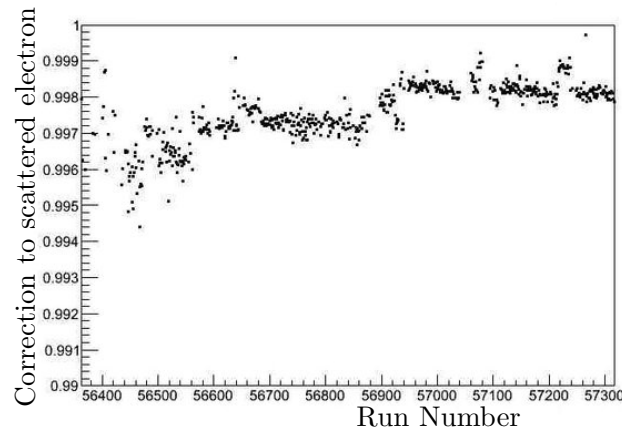


Figure 13: Plot of correction factor calculated for the entire *g12* run set

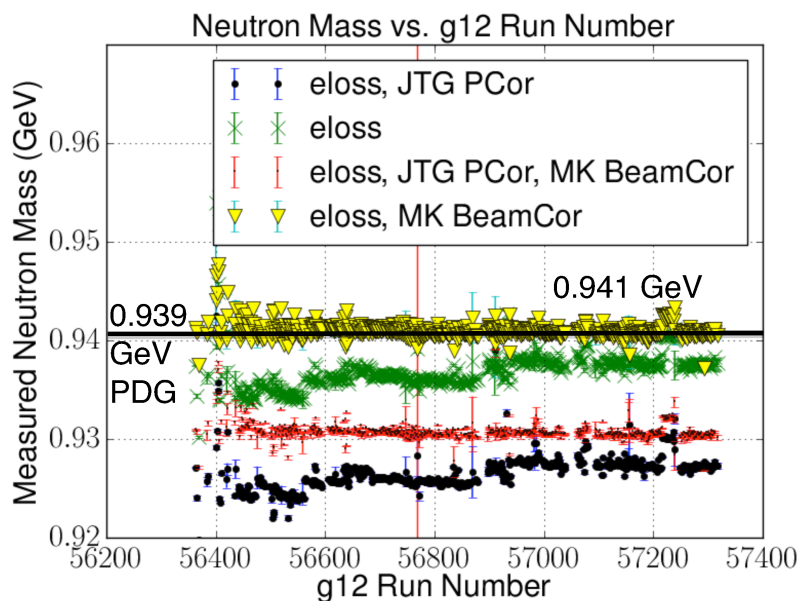


Figure 14: Plot of missing neutron mass using various corrections. The yellow triangles show a missing neutron mass with only “energy-loss” and beam correction applied (MK BeamCor) in which was the only corrections needed to correct the *g12* data stream. PDG mass for the neutron is 0.939565 GeV/c.

2.3 Start Counter Calibration and Resolution

The start counter time-walk calibration took into account the varying geometry of the paddles. Fig. 15 shows the uncorrected timing difference for paddle 3 (of 24) as a function of ADC while Fig. 16 shows the corrected timing. This was done for each paddle and the resulting resolutions can be seen in Fig. 17 for pions, Fig. 18 for protons, Fig. 19 for pions and all paddles, Fig. 20 for pions a function of beam energy and Fig. 21 for pions as a function of geometry. The run-by-run resolution can be seen in Fig. 22.

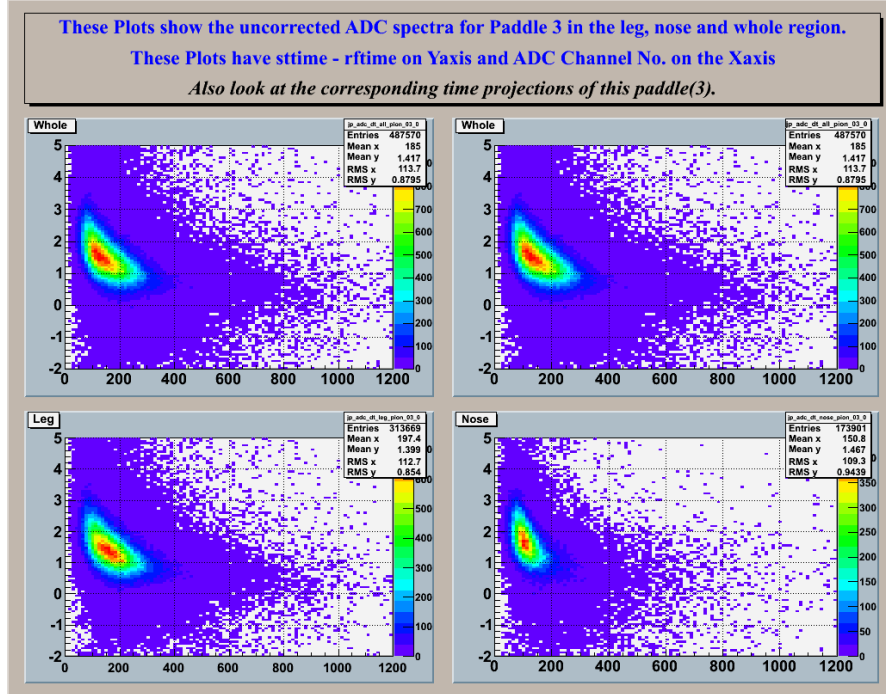


Figure 15

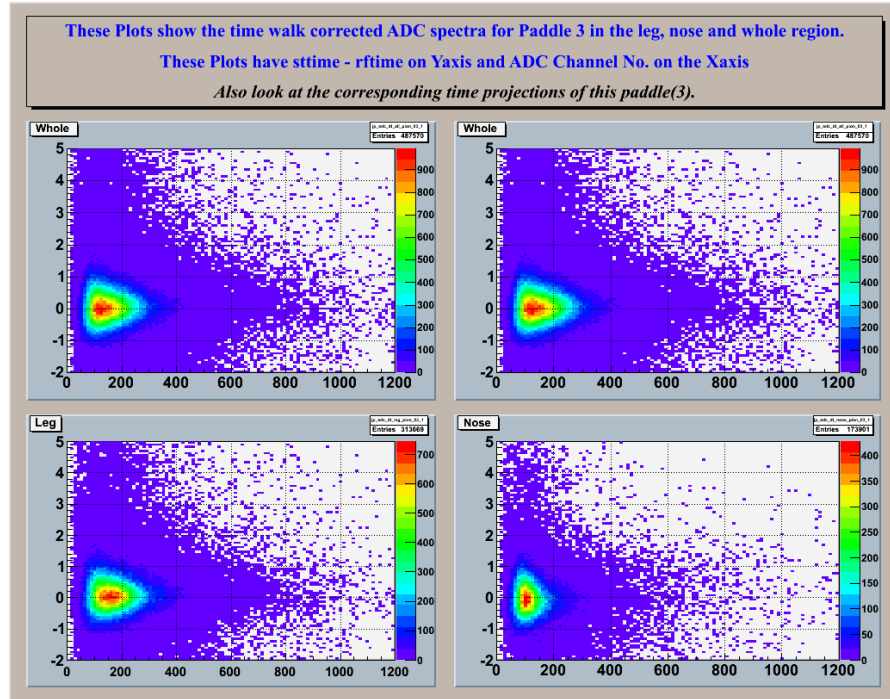


Figure 16

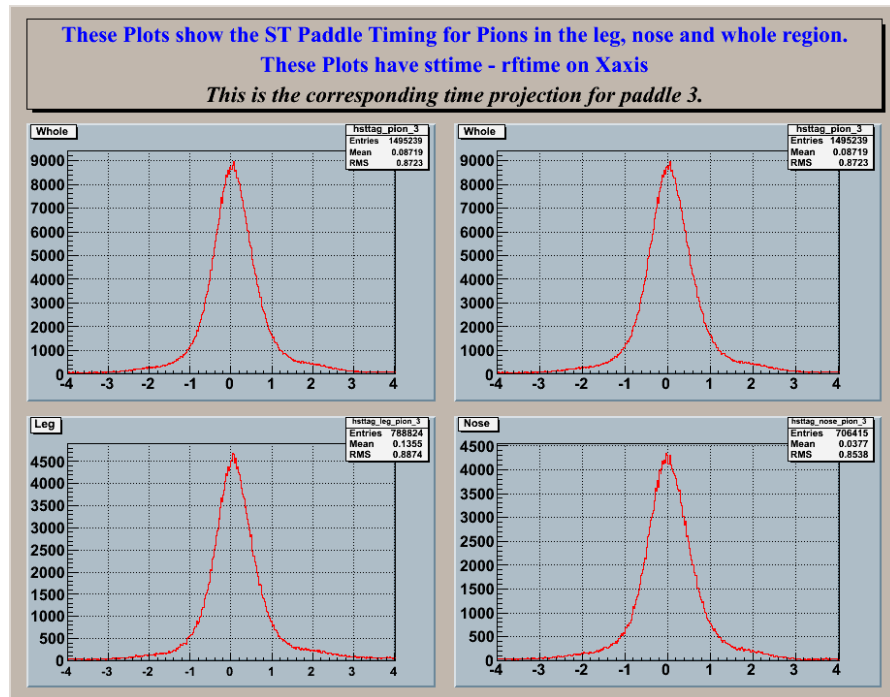


Figure 17

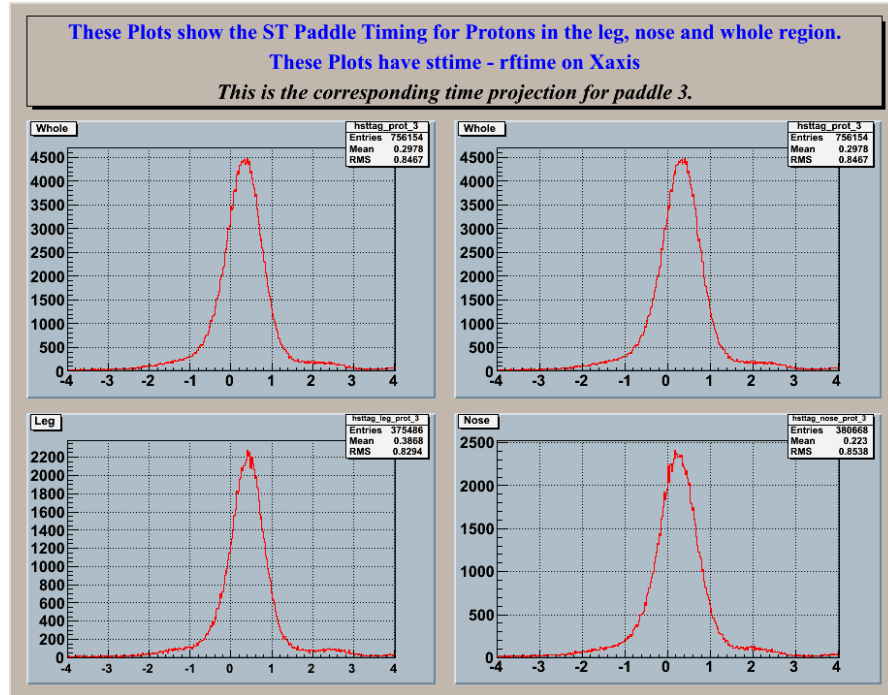


Figure 18

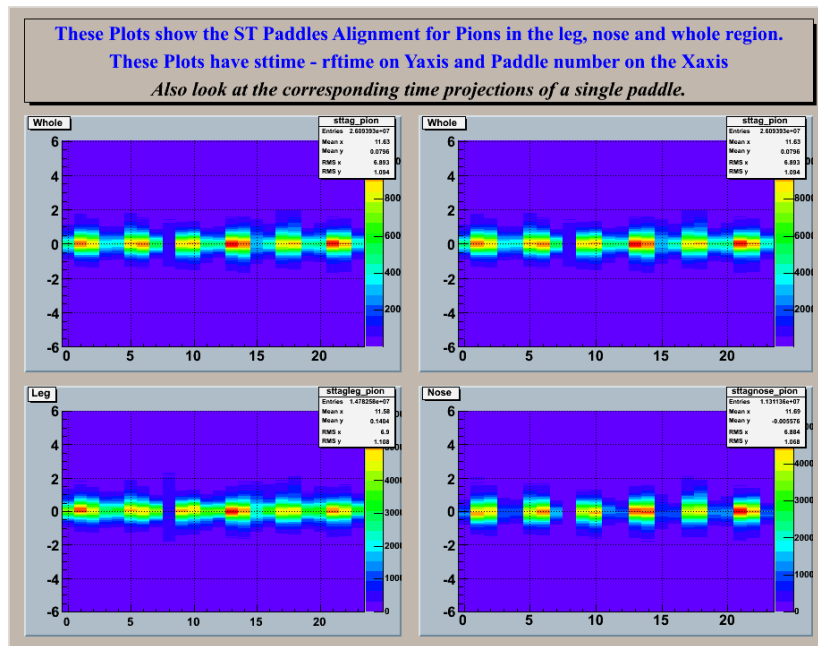


Figure 19

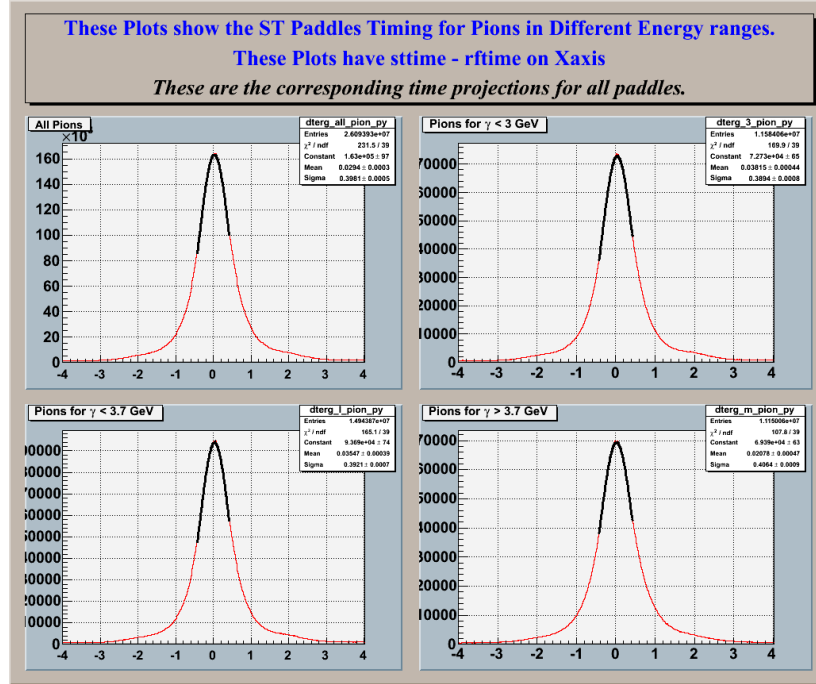


Figure 20

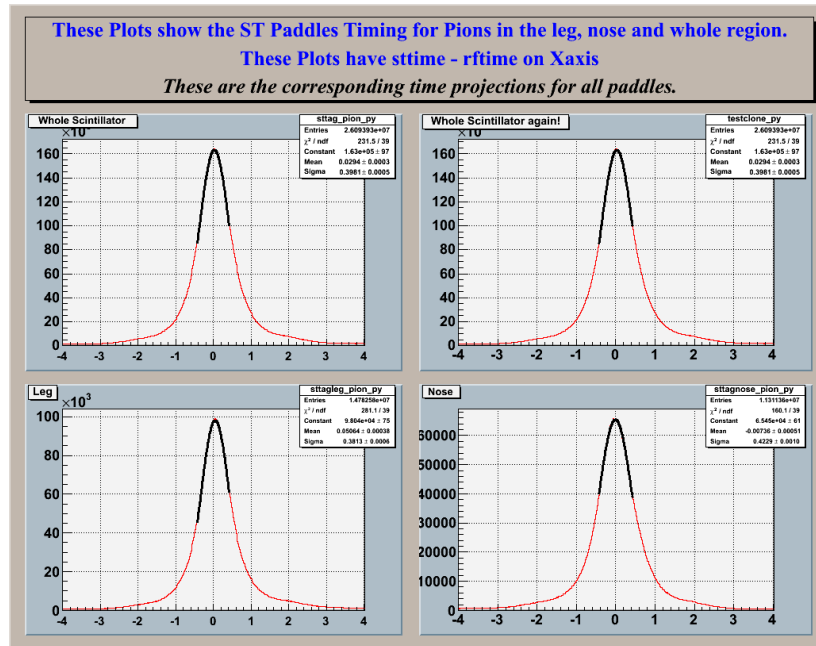


Figure 21

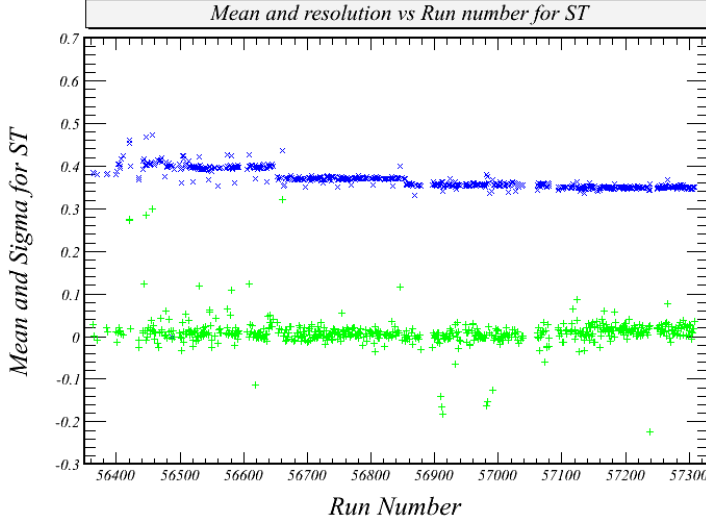


Figure 22

As a check on the timing resolution of the start counter, we used data containing at least two K^+ (this was part of the cascade baryon search) to look at kaons, pion and protons at the same time. The momenta (p) of the tracks was given by the drift chamber and tracking algorithm found in the TBTR bank, and the energy (E_{PID}) of the particle was set by particle identification. This allowed us to calculate the speed of the particle:

$$\beta_{\text{PID}} = \frac{p}{E_{\text{PID}}}. \quad (10)$$

This was used to calculate the vertex time of the particle:

$$t_{\text{vtx}}^{\text{TOF}} = t_{\text{TOF}} - \frac{\ell_{\text{TOF}}}{c\beta_{\text{PID}}}, \quad (11)$$

where t_{TOF} and ℓ_{TOF} are the time and path length of the track at the TOF plane as obtained from the TDPL bank. This time was converted to a “photon time” (t_{photon}) by subtracting the photon propagation time (t_{prop}) from the center of the target:

$$t_{\text{photon}}(\text{TOF}) = t_{\text{vtx}}^{\text{TOF}} - t_{\text{prop}}, \quad (12)$$

where

$$t_{\text{prop}} = \frac{1}{c} (z_{\text{tgt}} - z_{\text{vtx}}), \quad (13)$$

where z_{tgt} is the center of the target’s z-position (-90 cm in the CLAS coordinate system), and z_{vtx} is the z-coordinate of the track’s vertex position – in this case, the intersection of the two kaons where the covariance matrixes of the estimated momenta are taken into account through the standard MVRT vertexing algorithm. This photon time, $t_{\text{photon}}(\text{TOF})$, was compared to the RF-corrected tagger times ($t_{\text{TAG,RF}}$) of each hit in the photon tagger as obtained from the TAGR bank. The resulting data indicates a timing resolution of 310 ns for protons, 400 ns for pions, and 430 ns for kaons.

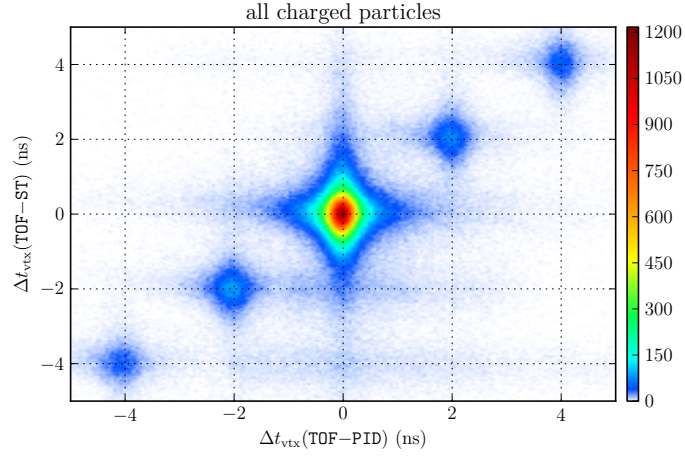


Figure 23: Difference in vertex times for each track for the two calculations made above. Represents 1.5% of the total statistics.

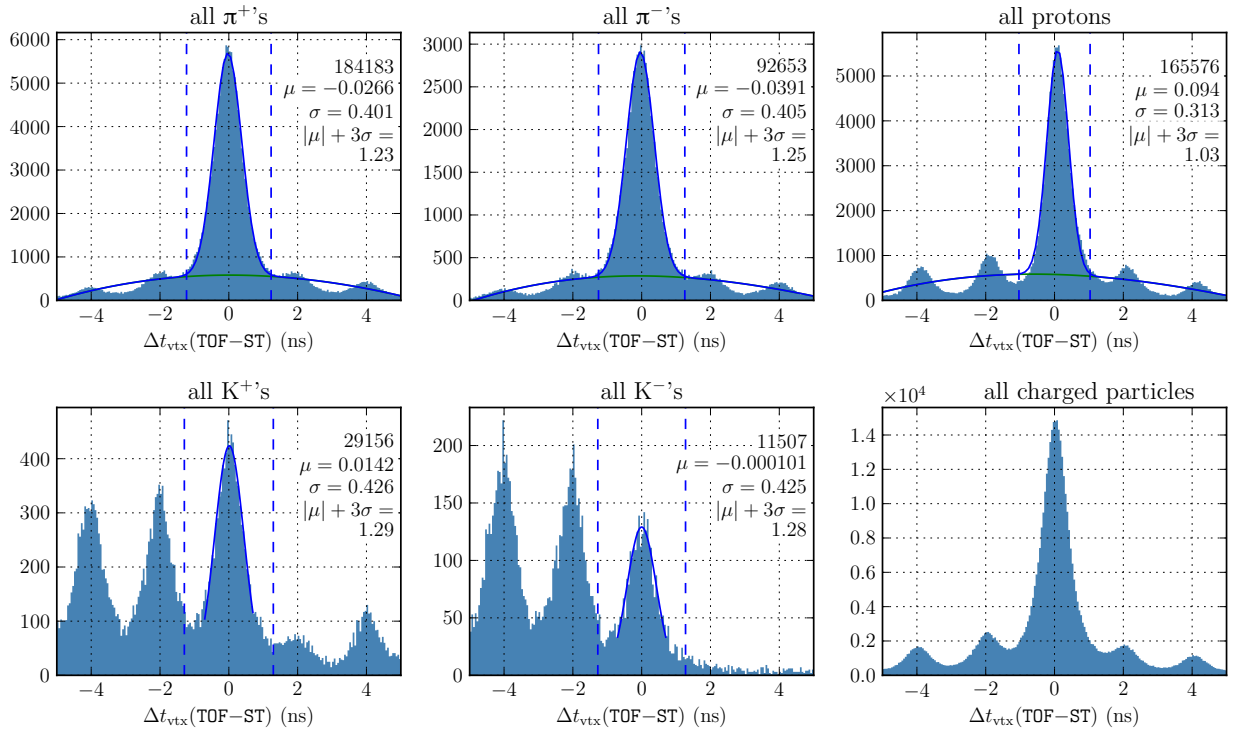


Figure 24: Difference in vertex time between that of the photon and of the tracks based on start counter and time-of-flight times. Represents 1.5% of the total statistics.

2.3.1 Start Counter Efficiency

2.4 Drift Chamber Calibration and Resolution

2.4.1 Drift Chamber and TOF smearing parameters in gpp

Tracking in the Drift Chamber of a CLAS Sector is performed using the six superlayers of the DC. A good measure of the the quality of tracking are the DC residuals for each superlayer. After a track is identified using the hit elements in the DC superlayer, It's DC residual is calculated using the TBLA bank as follows:

```
fabs(TBLA->tbla[i].fitdoca) - fabs(TBLA->tbla[i].calcdoca)
```

The values of the DC residuals in the CLAS data are empirically found to be a good fit to a convolution of 2 gaussians - a narrow gaussian and a broad gaussian. During DC calibrations efforts were made to minimise this residual to have maximum reconstruction efficiency. The mean and width of the residuals as a function of superlayer and run number are shown in Figs. 25 and 26 respectively.

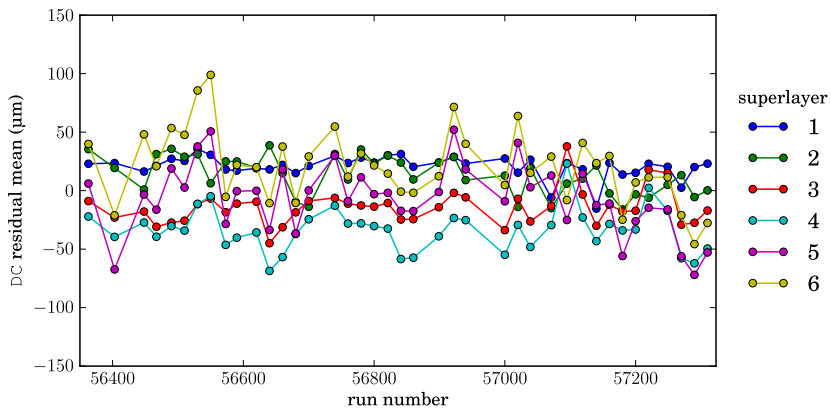


Figure 25: Mean of residuals for the drift chambers by superlayer and by run.

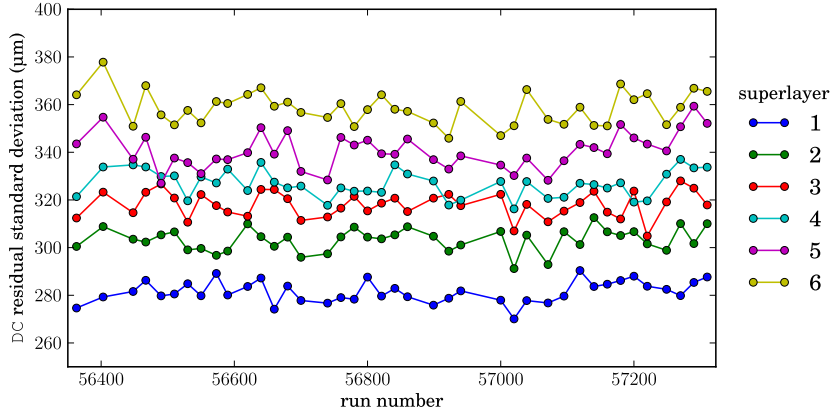


Figure 26: Gaussian width of residuals for the drift chambers by superlayer and by run.

2.4.2 Drift Chamber Wire Efficiency

2.5 Cerenkov Calibration and Resolution

2.5.1 Cerenkov Efficiency

2.6 Time-of-Flight Counter Calibration and Resolution

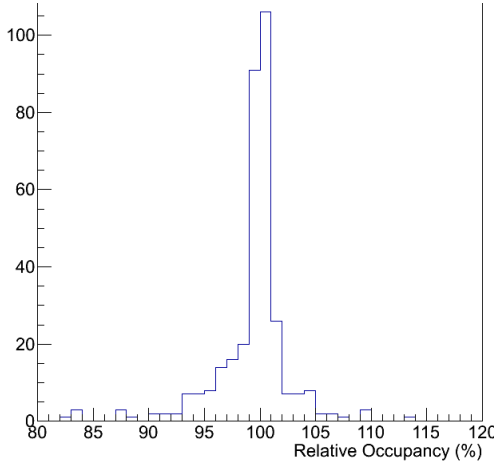
2.6.1 Time-of-Flight Counter Efficiency and Bad Paddles

As a standard procedure of the time-of-flight calibrations, the time-of-flight scintillators were initially studied during the calibration period, in which a list ^{*} of scintillators had a faulty ADC or TDC as shown in 11. Another study, as shown below, was conducted to determine the efficiency of each paddle and to reevaluate the status of their ADC and TDC. Due to the more stringent requirements of paddle efficiency in the study below, more paddles were considered to be faulty than in the initial study. 15 shows the additional paddles which were considered to be inefficient.

^{*}Can be obtained using the CLAS calibration database

Table 11: List of faulty paddles as compiled during calibration

Sector	SCID	Notes
1	6	No ADCR and TDCR
2	8	No ADCL and TDCL
2	34	No ADCL and TDCL
3	11	No ADCR and TDCR
3	57	No ADCL, ADCR, TDCL, and TDCR
4	48	No ADCL and TDCL
5	57	No ADCL, ADCR, TDCL, and TDCR
6	5	No ADCR and TDCR

**Figure 27:** Relative occupancy of all scintillators**Table 12:** Paddles below two and three standard deviations from the mean relative occupancy

	$2\sigma = 92.49\%$	$3\sigma = 89.05\%$
Sector 1	35 (91.20%)	40 (87.87%), 41 (82.63%), 56 (83.37%)
Sector 2	2 (92.38%), 35 (90.11%), 50 (91.99%)	41 (87.31%), 56 (87.98%)
Sector 3	35 (90.59%)	40 (88.98%), 41 (83.29%)
Sector 4		41 (83.61%)

To determine efficiency of each scintillator paddle, the number of hits [†] registered by every paddle was recorded [‡]. The relative occupancy of paddle i in sector j is defined the following way: list the number of hits recorded by all paddle i 's in sectors $\neq j$ and remove the ones with the most and least hits from the list. Take the average number of hits of the remaining three paddles. The relative occupancy is defined as

$$100 \times \frac{\text{Number of hits in paddle } i \text{ of sector } j}{\text{Average of remaining three paddles}} \%$$

[27](#) shows the relative occupancy of all scintillators plotted on a single histogram. A paddle is defined as inefficient if it is greater than two standard deviations below the mean relative occupancy of all scintillators. [12](#) shows the paddles which are below two (left) or three (right) standard deviations below the mean relative occupancy.

2.6.2 ADC and TDC Values

The occupancy alone is not enough to determine which scintillators are bad. The ADC and TDC values for all scintillators were also recorded and studied. [28](#) shows the ADC and TDC values for all scintillators. Some of the events registered had an ADC or TDC value of zero or a maximum ADC value (shaded in

[†]The data used were obtained from the `clas_0[run#].A01` files located in `/mss/clas/g12/data/`

[‡]This was done by using `bosdump -GSC` and parsing its output

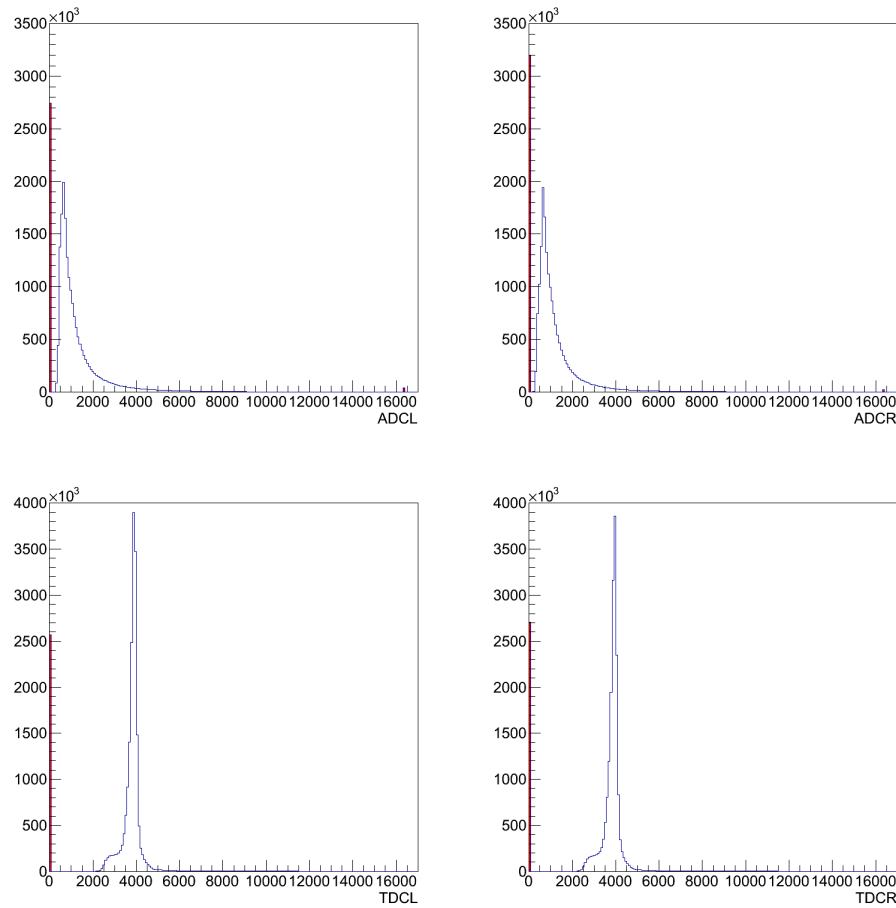


Figure 28: Top: ADC values of all scintillators. Left ADC (ADCL) values are on the left and right ADC values are on the right (ADCR). Shaded in red are events recorded with an ADC value of zero or maximum. Bottom: Same as Top but for TDC values

Table 13: Paddles which registered an ADC or TDC value of zero greater than 50% and 45%, respectively, of its entries

% Events with ADCL or ADCR = 0 > 50%		% Event with TDCL or TDCR = 0 > 45%
Sector 1	6 (100% ADCR)	6 (100% TDCR), 46 (97.89% TDCL), 50 (98.11% TDCL)
Sector 2	8 (100% ADCL), 34 (100% ADCL), 44 (50.22% ADCL), 54 (52.00% ADCR)	8 (100% TDCL), 34 (100% TDCL), 44 (47.51% TDCL), 54 (47.10% TDCR)
Sector 3	11 (100% ADCR), 56 (74.75% ADCR)	11 (100% TDCR), 56 (62.79% TDCR)
Sector 4	48 (100% ADCL)	48 (100% TDCL)
Sector 5	48 (77.98% ADCL)	48 (76.10% TDCL)
Sector 6	5 (100% ADCR), 56 (59.30% ADCR)	1 (98.78% TDCL), 5 (100% TDCR), 33 (97.78% TDCL)

Table 14: Union of ?? (Recommended list of paddles to knockout)

Sector 1:	6, 35, 40, 41, 50, 56
Sector 2:	2, 8, 34, 35, 41, 44, 50, 54, 56
Sector 3:	11, 35, 40, 41, 56
Sector 4:	41, 48
Sector 5:	48
Sector 6:	1, 5, 33, 56

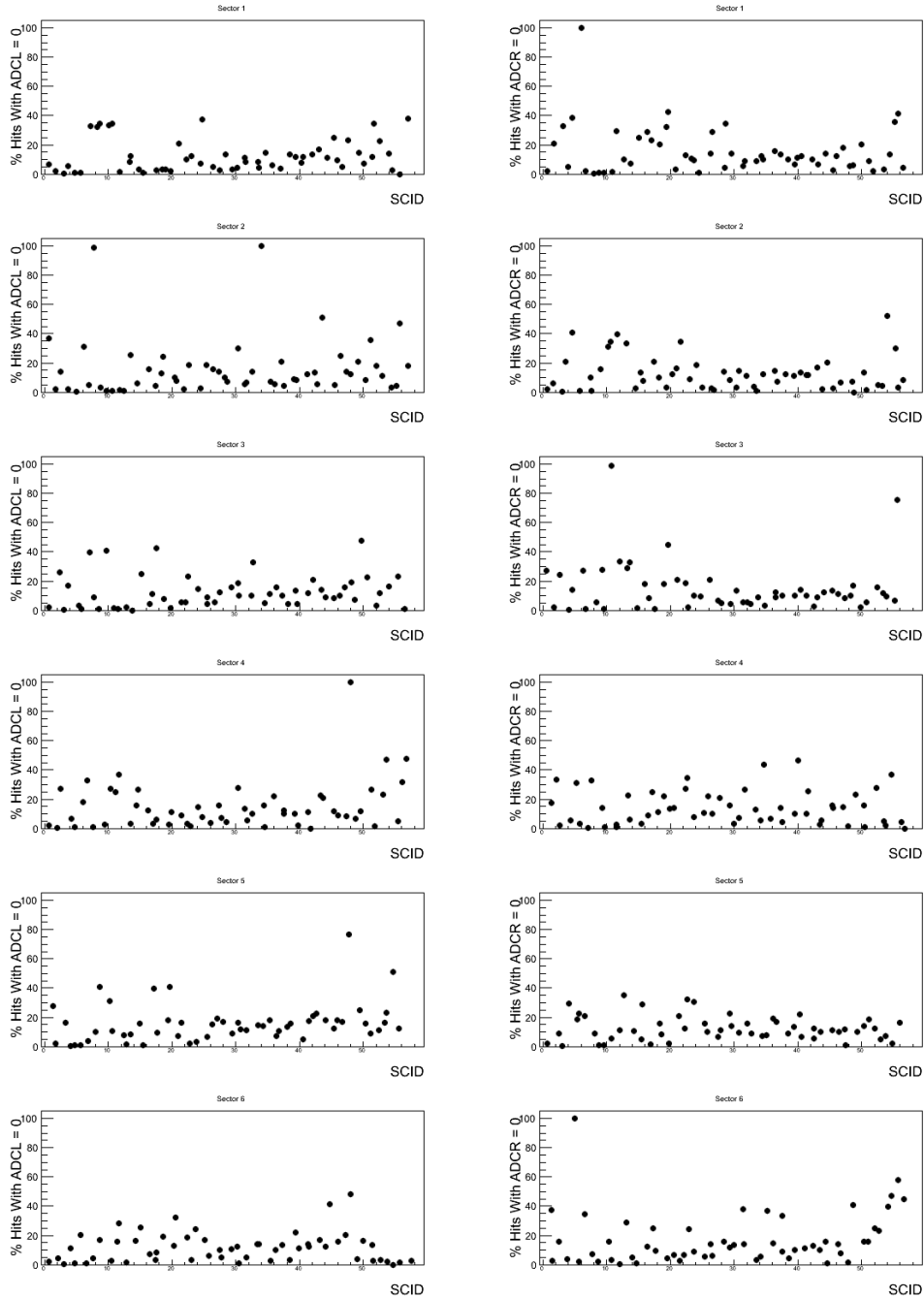
red). The percentage of events a scintillator recorded either a TDC or ADC value of zero or maximum ADC value was studied as shown in ???. ?? assisted in determining bad paddles. It (is to be) was decided that a paddle cannot have more than 50% of its ADC (left or right) values be equal to zero or more than 45% of its TDC (left or right) values equal to zero. 13 shows which paddles fall in these categories. 14 shows which scintillators should be knocked out due to low occupancy or too many null ADC or TDC values. Due to the small number of events in which a maximum ADC value is obtained, it is not recommended in knocking paddles out based on this measure. However, 16 shows the paddles which attain a maximum ADC value on more than 2.5% of its registered events.

Table 15: Paddles in 14 not included in 11

Sector 1:	35, 40, 41, 50, 56
Sector 2:	2, 35, 41, 44, 50, 54, 56
Sector 3:	35, 40, 41, 56
Sector 4:	41
Sector 5:	48
Sector 6:	1, 33, 56

Table 16: Paddles with percentage of hits registering a maximum ADC value > 2.5% of its events

Sector 1: 20 (2.93% ADCL)
Sector 3: 20 (4.26% ADCL)

**Figure 29:** Percentage of hits registering an ADC value of 0 for all scintillators. Left ADC (ADCL) are on the left and right ADC (ADCR) values are on the right

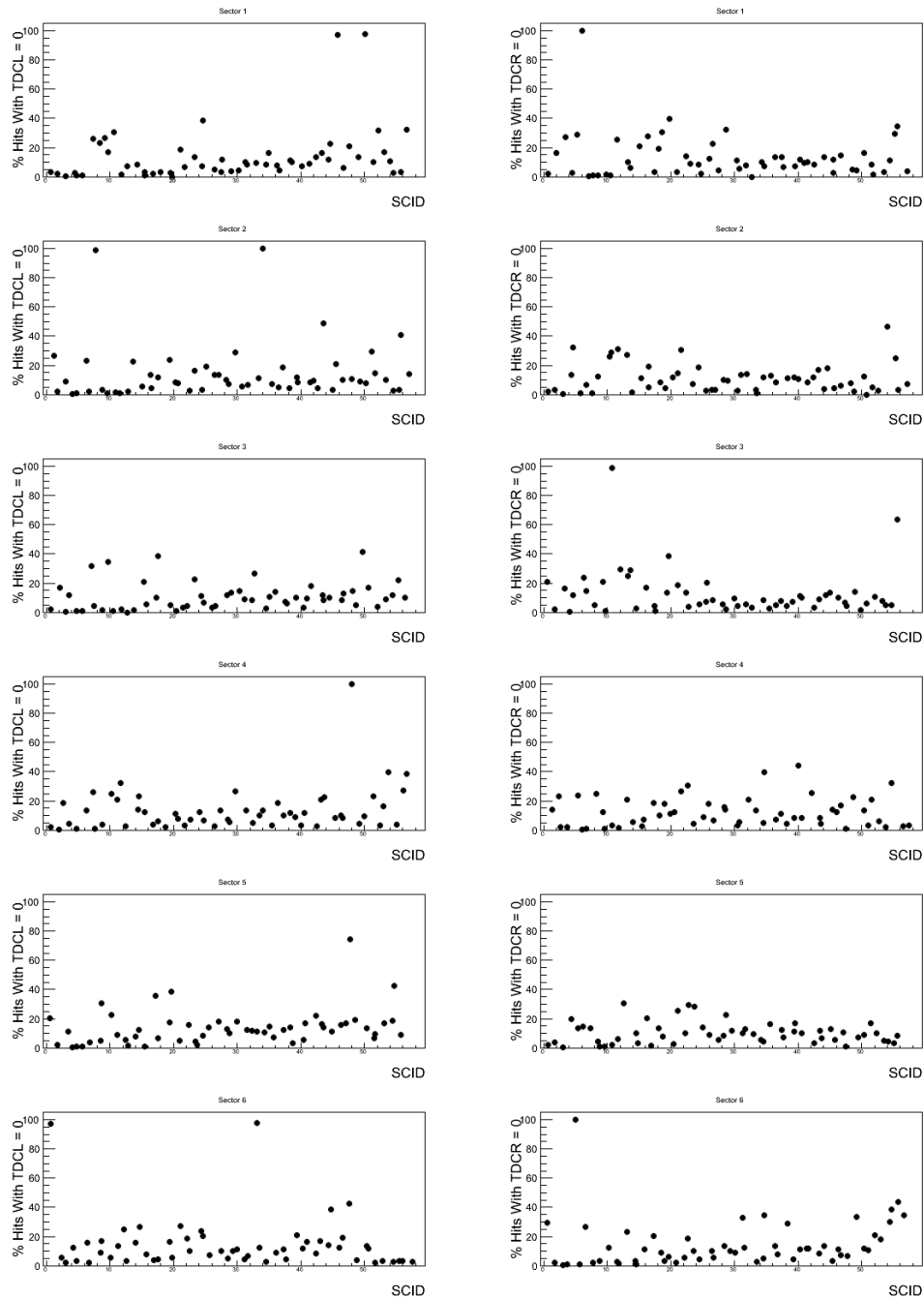


Figure 30: Percentage of hits registering an TDC value of 0 for all scintillators. Left TDC (TDCL) are on the left and right TDC (TDCR) values are on the right

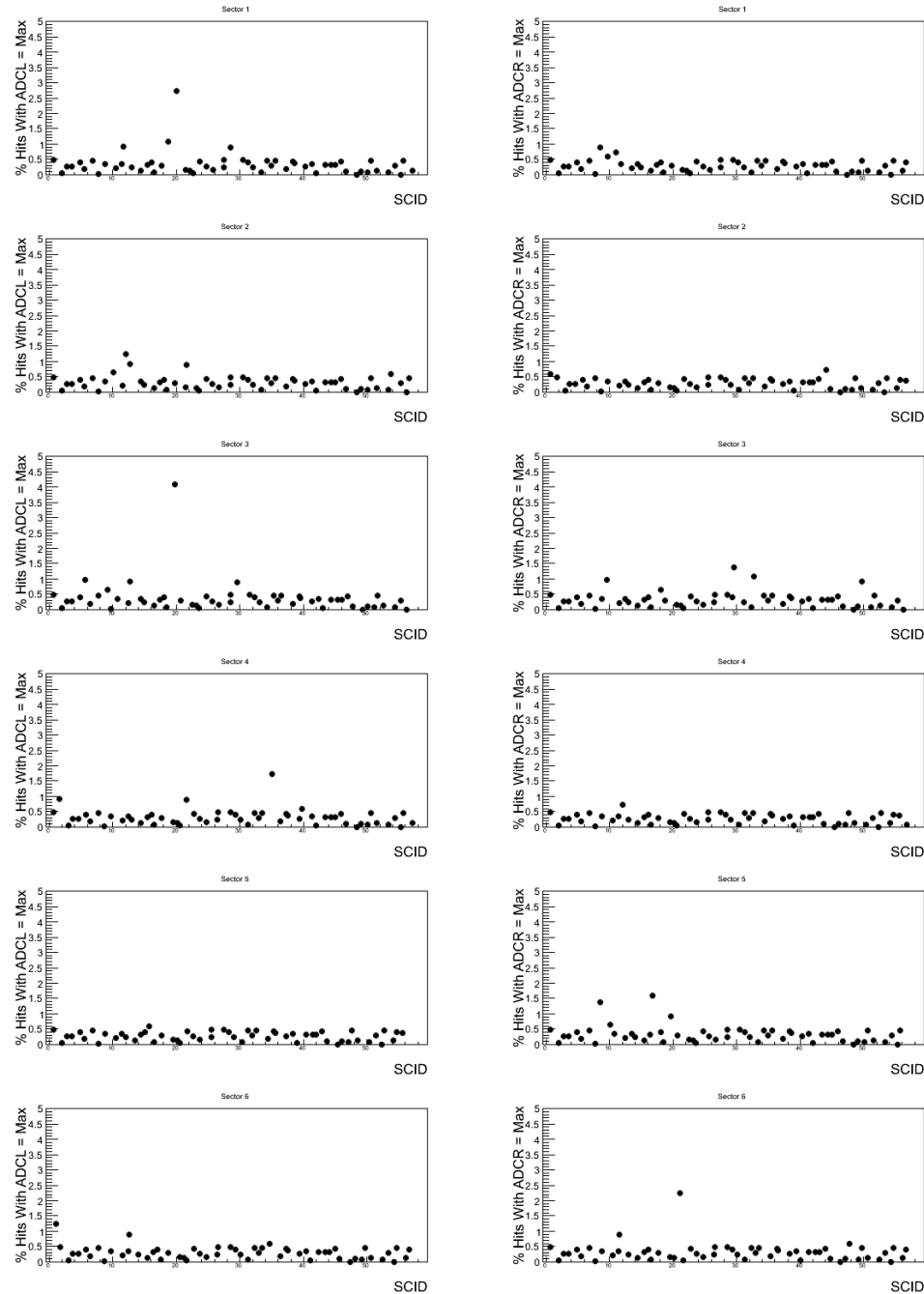


Figure 31: Percentage of hits registering a maximum ADC value for all scintillators. Left ADC (ADCL) are on the left and right ADC (ADCR) values are on the right

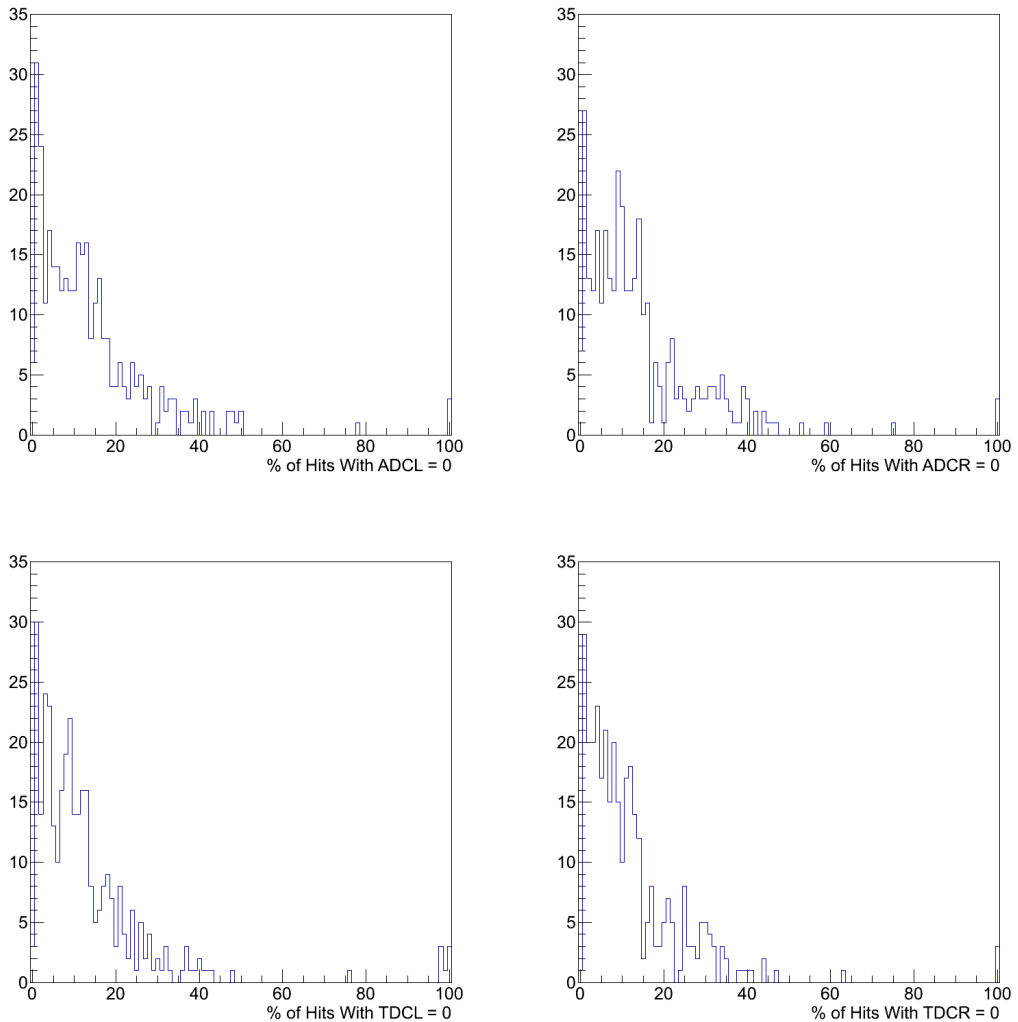


Figure 32: Top: Y axis projections of 29. Bottom: Y axis projections of 30

2.7 Electrocalorimeter Calibration and Resolution

2.7.1 Electrocalorimeter Efficiency and Bad Paddles

3 Procedure for Data Analysis

The broad steps for analysis of a specific reaction in the *g12* data are:

1. determine event selection cuts to be used on a small subset of the data,
2. skim the “cooked” data and produce an ntuple which will include the four-momenta and a few other parameters needed for the final analysis,
3. tune the analysis on the data to get the final yields,
4. run simulations through the tracker/digitizer (`gsim`), smearing (`gpp`), track reconstruction (`a1c`), and the final analysis programs to obtain efficiencies and acceptances,
5. calculate the beam flux corresponding to the data analyzed,
6. tie the yields, acceptances and flux together to come up with a final answer and an absolute scaling.

One or more of these steps, or parts of these steps, may not be necessary for a given analysis and they do not have to be done this order. This section discusses where to find the various programs and files needed for each of these steps.

3.1 “Pass1” Cooking and Data Reconstruction

This section describes the process of reconstructing the raw data into almost-physics-ready form. Broadly speaking, the output of this procedure is the three-momenta of the detected final-state particles and various supporting measurements such as timing or energy deposit which is used for particle identification.

The reconstruction program `a1c` requires an environment variable to point to the correct run index for this run period. This can be set in a bash shell using the command:

```
export CLAS_CALDB_RUNINDEX=calib_user.RunIndexg12
```

The command to cook the `gsim` bos file using the `a1c` program is:

```
a1c -T4 -sa -ct1930 -cm0 -cp0 -X0 -d1 -F -P0x1bff -z0,0,-90 \
-Aprlink_tg-90pm30.bos -o3pi.a1c 3pi.gpp
```

which will produce BOS files similar to the “cooked” data mentioned above in Sec. ???. This is the same command to be used to *recook* raw data files.

There was only one “physics” pass of the *g12* data, labeled `pass1`, which represents 99% of the reconstructable data taken. It was determined that tracking down that last 1% was not worth the effort. On JLab’s common user environment (CUE), the cooked data can be found here:

```
/mss/clas/g12/production/pass1/bos
```

and the raw data can be found here:

```
/mss/clas/g12/data/
```

Please see JLab's SciComp help pages on how to get these files off the mass storage system. The source code for pass1 was consistent with revision 4715 in the Subversion repository found here:

<https://jlabsvn.jlab.org/svnroot/clas/trunk>

which was linked against the 2005 version of the CERNLIB.

3.2 Obtaining Reconstructed Data

All reconstructed data resides in BOS files on the tape-silo at JLab under the directory:

```
/mss/clas/g12/production/pass1/bos
```

which contains the following subdirectories or “categories” used for event-sorting:

1-1ckaon1ctrk Events which have at least 2 charged tracks, one of which is a “possible kaon.” A possible kaon is either a track that the PART bank says is a kaon, or a high-momentum charged pion ($> 2.0 \text{ GeV}$), or a really high momentum proton ($> 3.0 \text{ GeV}$). The idea of this selection is to leave no kaon behind.

2-2pos1neg_not_1ckaon1ctrk Two-positive and one-negative (+ + −) inclusive events which are *not* included in *1-1ckaon1ctrk*. So, for example, if you wanted all (+ + −) events you would have to use both this category and *1-1ckaon1ctrk*.

3-2ctrk_not_2pos1neg_1ckaon1ctrk Events with 2 or more charged tracks which do not qualify for either *1-1ckaon1ctrk* or *2-2pos1neg_not_1ckaon1ctrk*.

4-not_2ctrk_2pos1neg_1ckaon1ctrk Physics events that do not fit into categories 1, 2, or 3.

5-other Non-physics events which may include scalers and such.

6-1lepton Redundant set of all events with a single “possible lepton” according to the

```
ClasParticle::isMaybeLepton()
```

method in the ClasEvent analysis suite.

7-4ctrk Redundant set of all four-charged track events.

8-ppbar Redundant set of all proton, anti-proton events according to the PART bank.

Note that the first five of these categories are *mutually exclusive and complete* while the last three are completely redundant and are provided for convenience.

This bears repeating since it is a non-standard sorting of the cooked data: The five categories numbered 1 through 5 listed above consist of one and only one of *every* event recorded by the data aquisition during the g12 run period for the set of run which were deemed “good.” A specific single event will only be found in one of the first five categories. If you want to run on events that are described by category number 4 for example, you will have to include the data in categories 1 through 3 since these will also satisfy category 4 by design and by definition.

Typical analyses with *g12* will start with the particles as identified in the PART bank as default in the ClasEvent analysis suite. This provides the basic four-momenta of the tracks and their identification which is based on mass calculated from the time-of-flight. The photon associated with the event is then taken from the TAGR bank and the one closest in-time with the tracks is usually taken.

For a deeper analysis, one can get information for specific hits in a given subsystem by following the pointers in the PART and TBID bank to the TBTR, SCRC, ECHB or other similar banks. Most of the relavent banks needed for this type of investigation are included in the cooked data though several raw banks were dropped to save space. To recover the missing banks one would have to go back to the raw data and recock using the a1c program though we anticipate this will be a rare event.

3.3 *g12*-Specific Corrections

3.3.1 Final-State Particle Momentum Corrections

The event reconstruction of a particle track in CLAS starts in region 1 of the DC after the track has gone through the target and start counter. To reconstruct the track back to the event vertex, additional energy loss from the target and start counter are included. The standard CLAS ELOSS package provides the required functionality as detailed in Ref. [eloss]. ELOSS corrects for the energy lost as charged tracks go from the event vertex through the beam pipe, target, and start counter using the Bethe-Bloch equation [PDG] to relate the material characteristics and path length to energy loss.

The momenta of the tracks as measured by the Drift-Chamber (DC) have a systematic shift within each sector as a function of azimuthal-angle ϕ of one of the tracks. This can be seen in the “tranverse momentum balance” plots shown in Fig. 33. The transverse momentum balance for a given particle is defined as the sum of the momentum of the other particles projected onto the line that is perpendicular to the beam having the same ϕ angle as the given particle minus its momentum transverse to the beam.

The final *g12* momentum corrections are in the clas6 trunk:

```
svn co https://jlabsvn.jlab.org/svnroot/clas/trunk/pcor/g12pcor
```

The code to use the momentum corrections should look something like this:

```
#include "g12_pcor.hpp"

string parms_dir = "/group/clas/parms";

/// load up momentum correction parameters
clas6::g12::MomentumCorrection Pcor(parms_dir);

///begin loop over charged particles
{
```

Figure 33: Transverse momentum balance of exclusive $p \pi^+ \pi^-$ events as a function of azimuthal angle ϕ of each track before momentum corrections.

Figure 34: Transverse momentum balance of exclusive $p \pi^+ \pi^-$ events as a function of azimuthal angle ϕ of each track after momentum corrections.

```
    float newp = Pcor.pcor(oldp, phi, geant3_pid);  
}
```

Where geant3 pid is the particle ID (according to geant3) for π^+ , π^- , p, K^+ or K^- .

A simultaneous fit was done by adding a correction to the momenta of each particle for each sector which was linear in ϕ . The result of the correction is shown in Fig. 34.

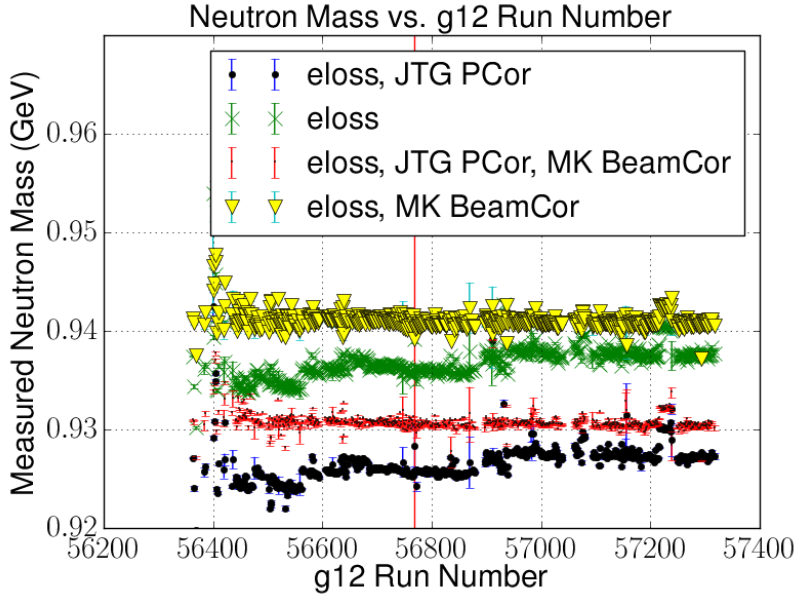


Figure 35: Neutron mass balance of exclusive $n\pi^+\pi^+\pi^-$ events as a function of run number for before corrections, momentum only, beam only, and after both beam and momentum corrections.

3.4 General Features of Lepton Data in *g12*

To identify electrons and positrons properly in CLAS, quantities obtained from the CC and EC are used to reject charged pions. The CC collects the number of photo-electrons caused by Cherenkov radiation and the EC records the energy deposition of electrons/positrons as well as photons. A previous CLAS experiment *g7* analyzed the properties of medium modifications from the decay of vector mesons through the leptonic decay channel. This experiment derived a set of cuts for identifying electron/positrons pairs in CLAS by employing specific cuts to the number of photo-electrons (NPE) detected in the CC, a match in azimuthal angle ϕ from a charged track in the DC to the ϕ of the CC, as well as comparing the momentum of the charged track to the energy deposited in the EC. These cuts can be found in Table 17. To validate the

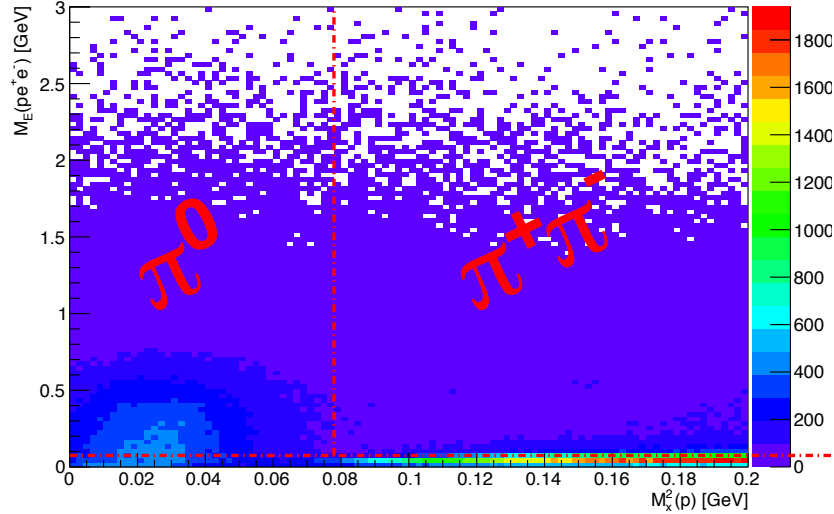
Table 17: Cuts applied to the CC and EC to perform electron/positron *PID*

Subsystem	Quantity	Cut
CC	# of photo-electrons (NPE)	$NPE > 2.5$
	$DC \phi & CC \phi$	$DC \phi = CC \phi$
EC	q^\pm momentum threshold (p_{thres}) & EC deposited energy (E_{calo})	$p_{\text{thres}}^{\text{high}} < E_{\text{calo}} < p_{\text{thres}}^{\text{low}}$

g7 electron/positron PID scheme for *g12*, a comparison of the CC and EC quantities was performed for all charged tracks CC/EC hit signatures and while selecting events from π^0 decay. To separate the π^0 events from the $\pi^+\pi^-$ events, all charged pions were assigned the mass of electrons and cuts were placed on the missing energy of $\gamma p \rightarrow p e^+ e^-$ as well as a cut on the missing mass squared of $\gamma p \rightarrow p$, values found in Table 18. A graphical depiction of the cuts applied to separate π^0 events from the $\pi^+\pi^-$ events is seen in Fig. 36. The

Table 18: Cuts applied to separate π^0 events from $\pi^+\pi^-$ events

Cut Topology	Topology Quantity	Value
$\gamma p \rightarrow pe^+e^-$	Missing Energy (M_E)	$> 0.075 \text{ GeV}$
$\gamma p \rightarrow p$	Missing mass squared (M_x^2)	$< 0.0779 \text{ GeV}^2$ for π^0 events $> 0.0779 \text{ GeV}^2$ for $\pi^+\pi^-$ events

**Figure 36: a**

nd $\pi^+\pi^-$ for PID Validation] Plot of missing mass squared of off proton (horizontal) vs. missing energy of proton e^+e^- (vertical). The red dashed vertical line depicts the $\pi^+\pi^-$ threshold mass cut while the horizontal red dashed line represents the missing energy cut-off used to separate $\pi^+\pi^-$ from π^0 .

values of the threshold momentum are calculated from empirical studies and are based upon calculations using the momentum obtained from the DC p under the following criteria;

$$\begin{aligned} p_{\text{thres}}^{\text{low}} &= \alpha p * (p + EC_{P_LO})/p \\ p_{\text{thres}}^{\text{high}} &= \alpha p * (p + EC_{P_HIGH})/p \end{aligned}$$

where $EC_{P_LO} = -0.3$, $EC_{P_HIGH} = 0.5$ and

$$\alpha p = \begin{cases} .23 * p + .071p^2 - .032p^3, & p < 1.0 \text{ GeV} \\ 0.272p, & p > 1.0 \text{ GeV} \end{cases}$$

3.4.1 CC Comparison

The NPE measured by the CC for all positron/electron (e^+/e^-) candidates can be seen in Fig 37. The sharp decline prior to 2.5 NPE is due to photo-electrons created by electron/positrons, pions traveling through the CC or pions producing delta-electrons which pass through the CC. Delta-electrons are created as an effect of

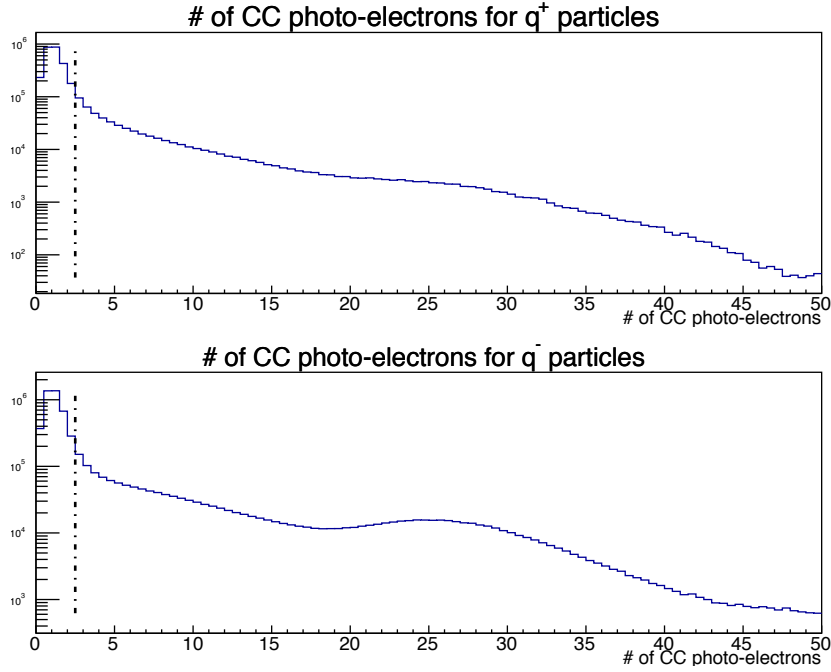
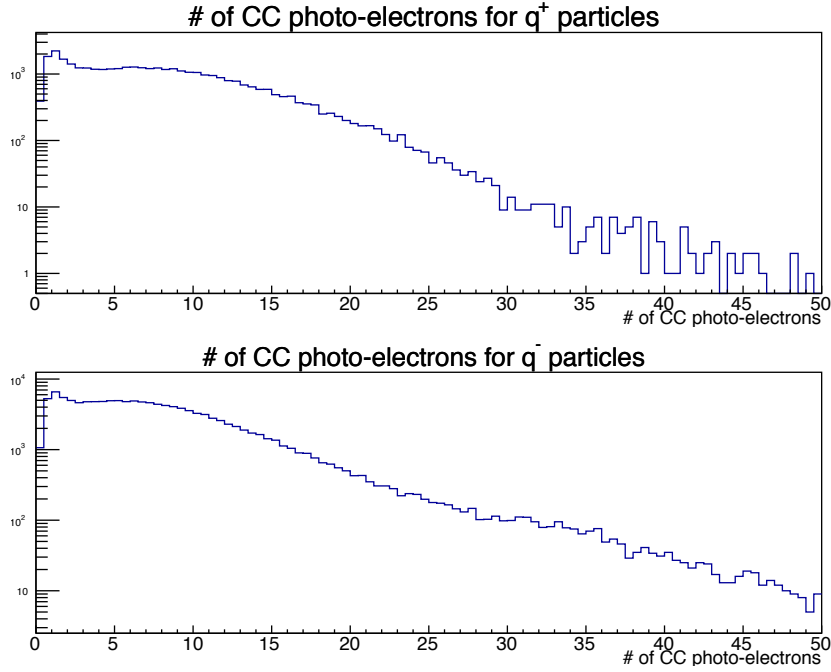


Figure 37: Plot of NPE measured by CLAS CC subsystem for positron/electron candidates top/bottom respectively. The dashed dotted vertical line depicts the cut applied if using the $g7$ lepton PID scheme.

the ionization of gases that could be present when the pion travels through the DC. These types of electrons are typically lower in momentum than the electrons obtained from particle decays in CLAS and thus according to eq. ?? should emit less NPE per unit length.

Through mass conservation the particles for the π^0 events must be e^+/e^- pairs. In comparison to fig. 37, fig. 38 plots the NPE measured by the CC for all e^+/e^- pairs for π^0 events selected as shown in fig. 36. It can be seen that the sharp decline prior to $NPE = 2.5$ is reduced leaving mostly electrons or positrons signatures in the CC concluding that the $g7$ CC NPE cut is valid for identifying e^+/e^- pairs while rejecting π^+/π^- pairs.

**Figure 38: E**

vents] Plot of NPE measured by CLAS CC subsystem when selecting π^0 events seen in Fig 36, positron/electron candidates top/bottom respectively.

3.4.2 EC Comparison

Similarly to the CC comparison, figures 39, 40, 43, 44 depict the $p_{\text{thres}}^{\text{low}}$ and $p_{\text{thres}}^{\text{high}}$ cuts listed in Table 17 for the q^- and q^+ tracks respectively. After π^0 event selection, seen in figures 41, 42, 45, 46, the bulk of e^+/e^- events reside within the region of the cut acceptance therefore it is evident that the $g7$ EC cuts are valid for identifying e^+/e^- pairs. The following four plots are for electron(e^-) PID validation of the $g7$ EC cuts described in Table 17.

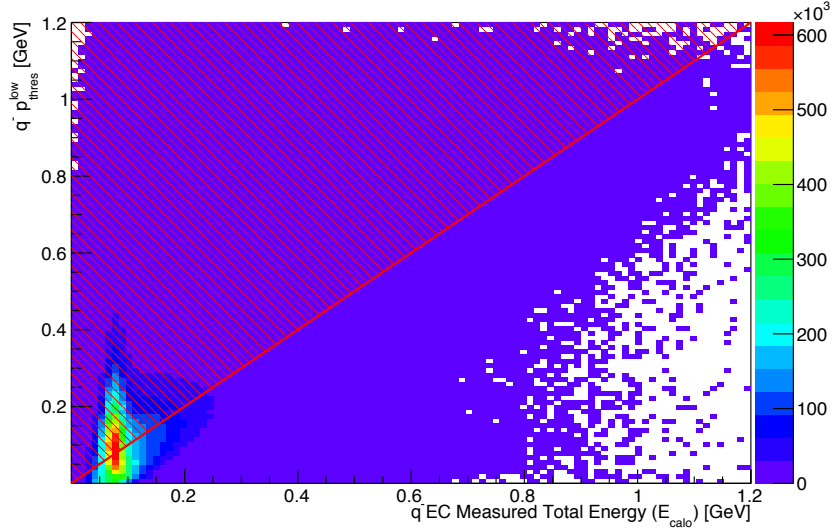


Figure 39: Plot of energy deposited measured by EC vs. track momentum $p_{\text{thres}}^{\text{low}}$ for negative charged tracks. The red region depicts the cut that would reject events in the $g7$ lepton EC PID scheme.

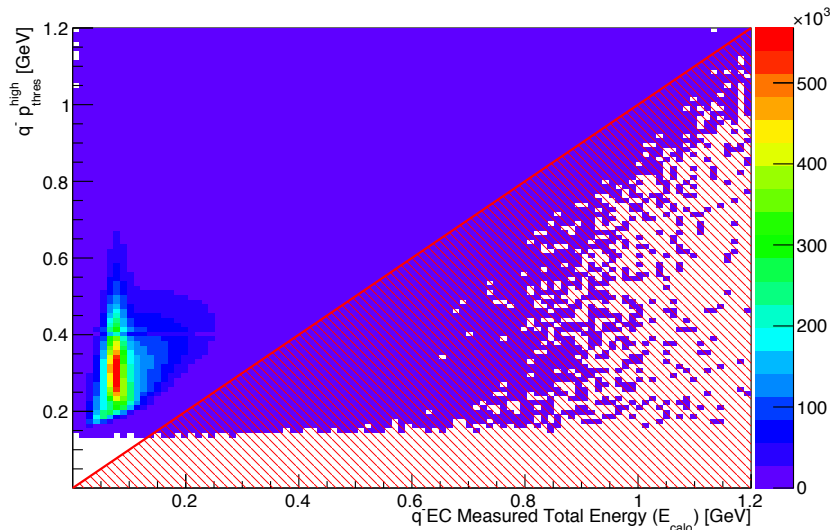


Figure 40: Plot of energy deposited measured by EC vs. track momentum $p_{\text{thres}}^{\text{high}}$ for negative charged tracks. The red region depicts the cut that would reject events in the $g7$ lepton EC PID scheme.

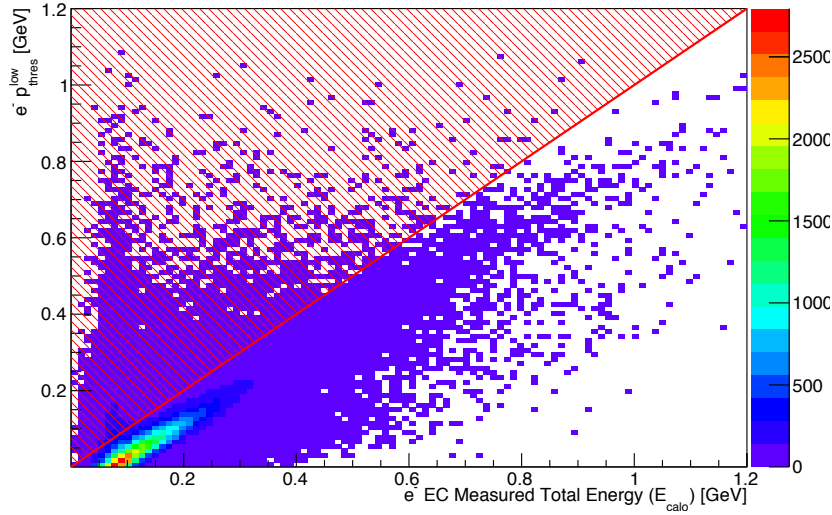


Figure 41: Plot of energy deposited measured by EC vs. track momentum $p_{\text{thres}}^{\text{low}}$ for electrons from π^0 events without the $g7$ lepton EC PID scheme applied. The red region depicts the cut that would reject events in the $g7$ lepton EC PID scheme.

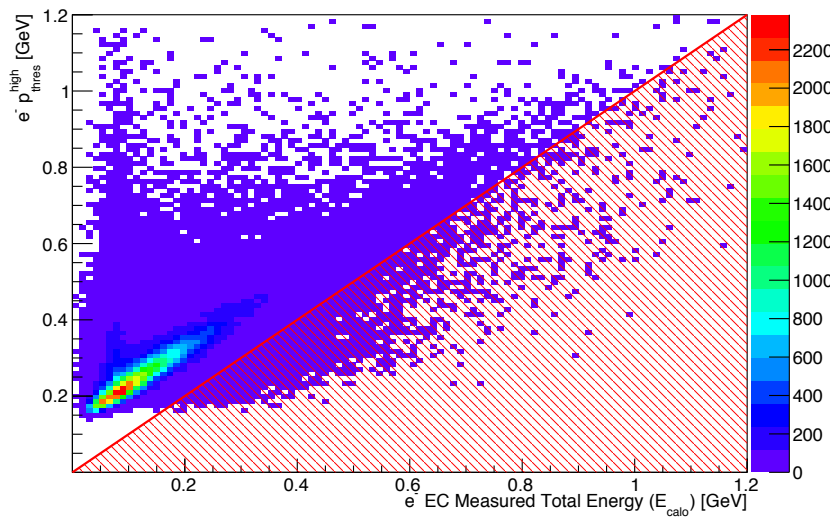


Figure 42: E

vents] Plot of energy deposited measured by EC vs. track momentum $p_{\text{thres}}^{\text{high}}$ for electrons from π^0 events without the $g7$ lepton EC PID scheme applied. The red region depicts the cut that would reject events in the $g7$ lepton EC PID scheme.

The following four plots are for positron(e^+) PID validation of the $g7$ EC cuts described in Table 17.

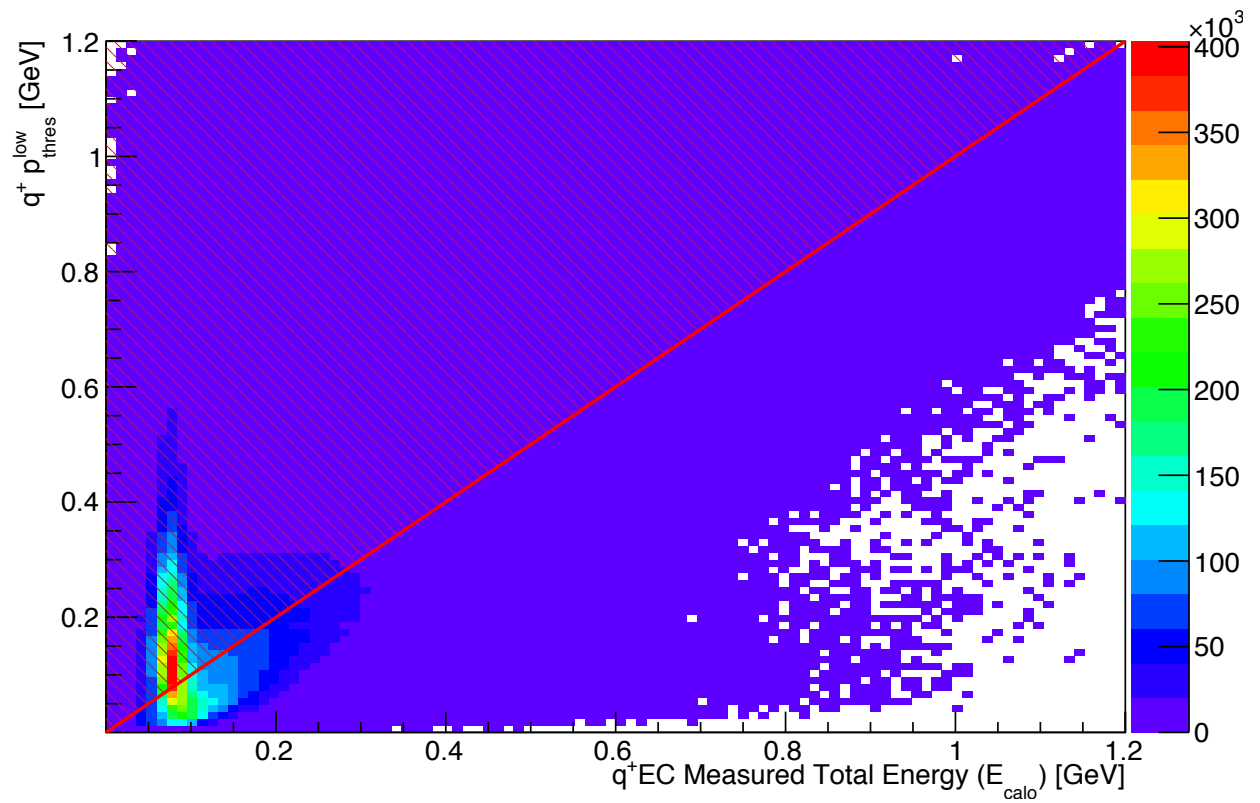


Figure 43: Plot of energy deposited measured by EC vs. track momentum $p_{\text{thres}}^{\text{low}}$ for positive charged tracks. The red region depicts the cut that would reject events in the $g7$ lepton EC PID scheme.

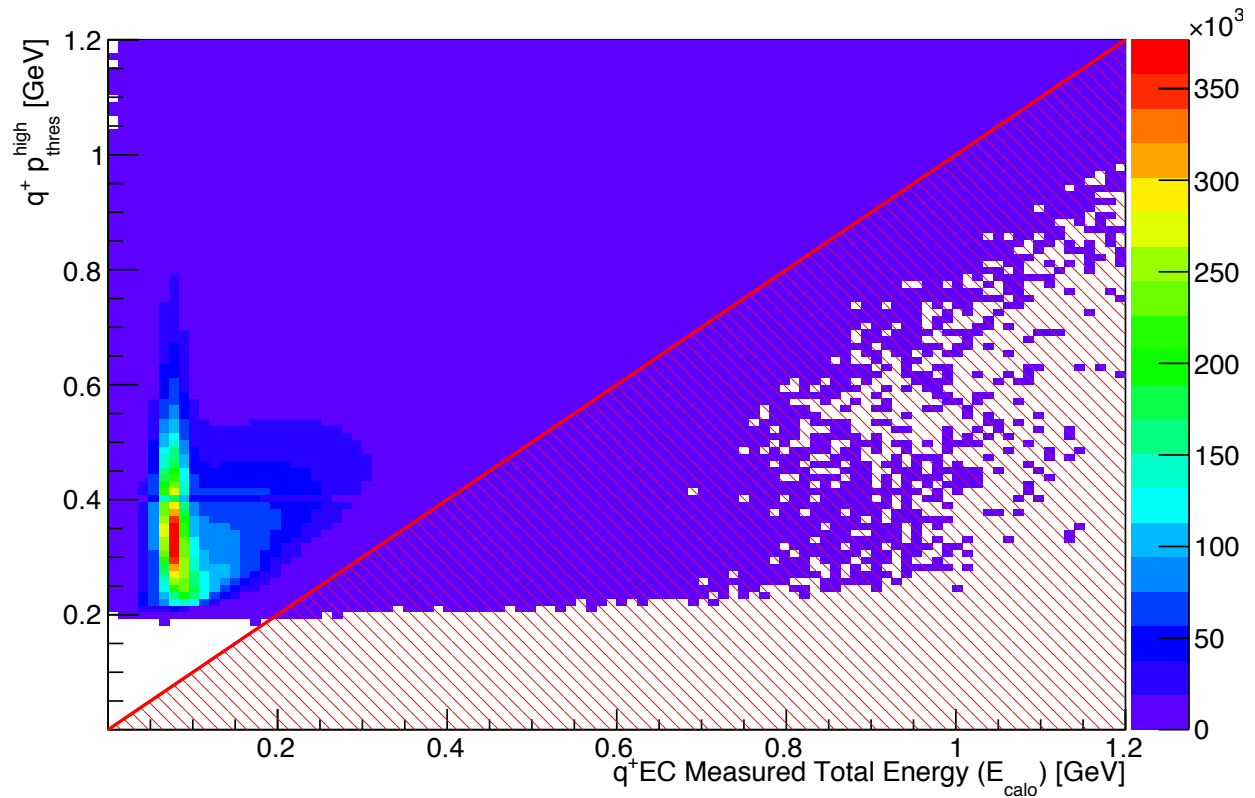


Figure 44: Plot of energy deposited measured by EC vs. track momentum $p_{\text{thres}}^{\text{high}}$ for positive charged tracks. The red region depicts the cut that would reject events in the $g7$ lepton EC PID scheme.

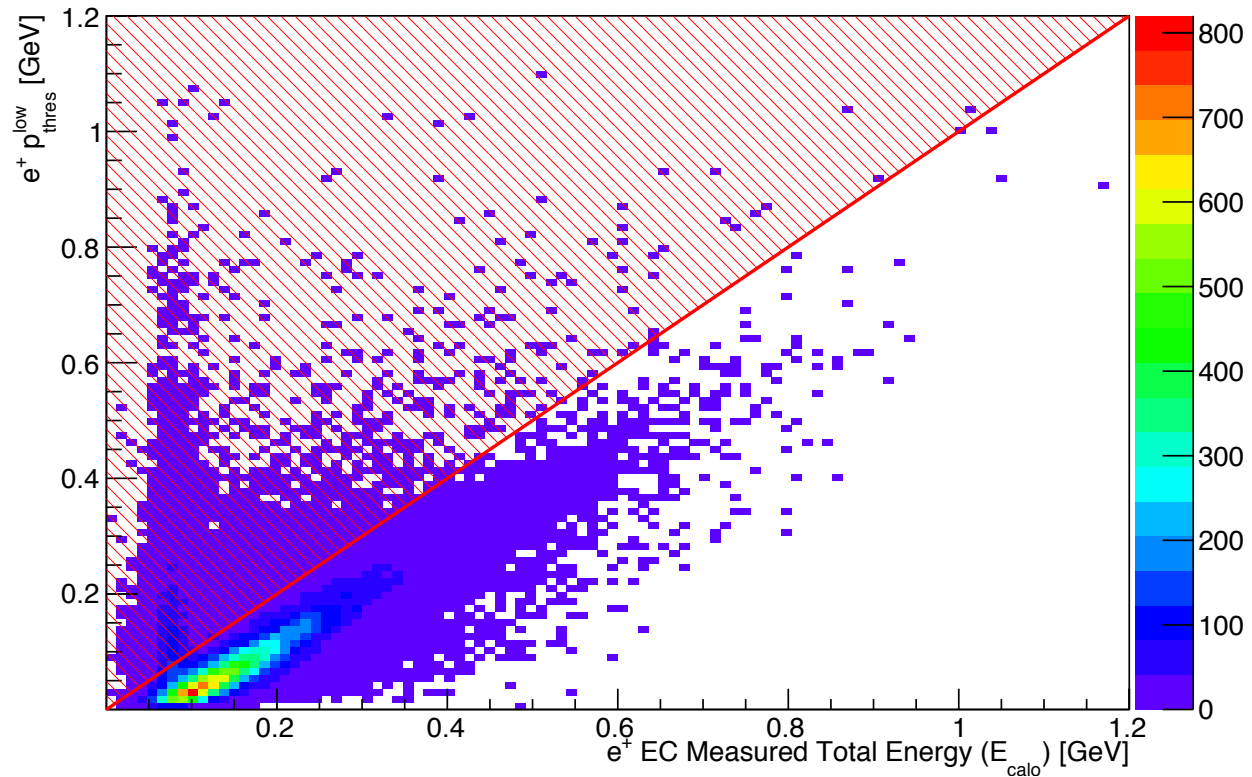
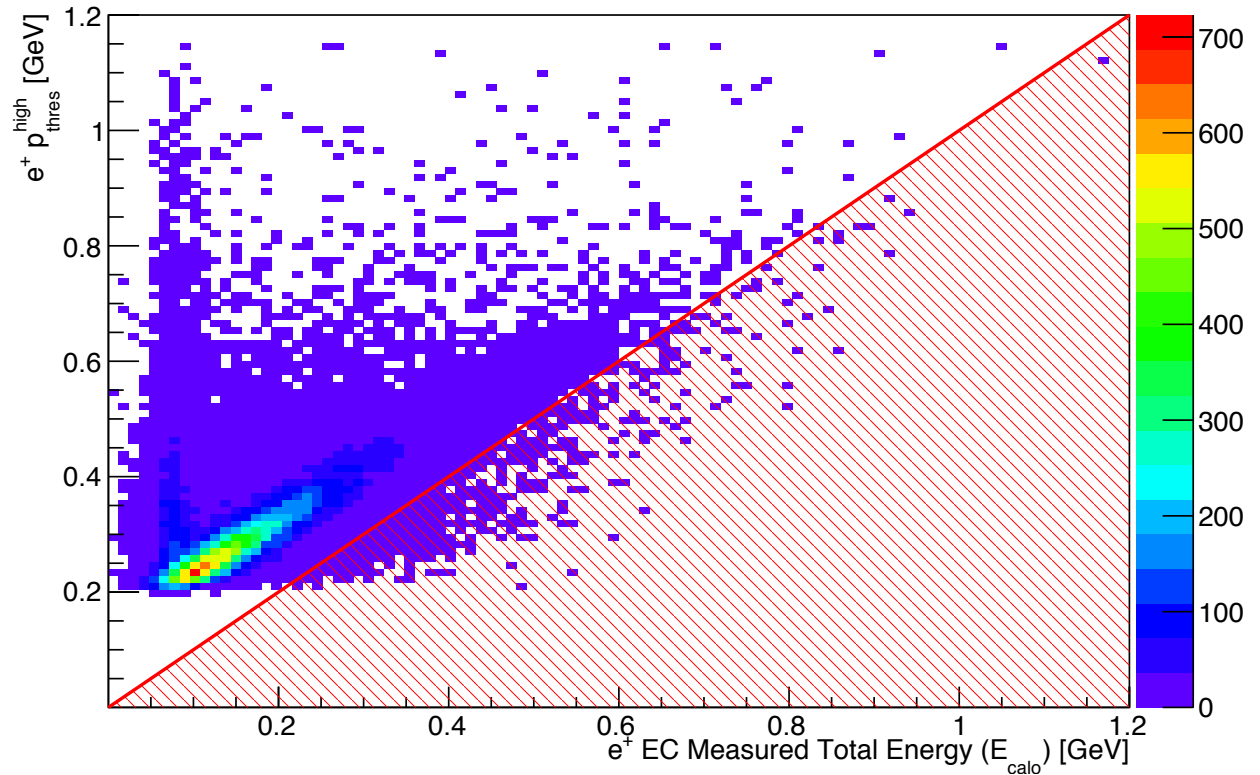


Figure 45: Plot of energy deposited measured by EC vs. track momentum $p_{\text{thres}}^{\text{low}}$ for positrons from π^0 events without the $g7$ lepton EC PID scheme applied. The red region depicts the cut that would reject events in the $g7$ lepton EC PID scheme.

**Figure 46: E**

vents] Plot of energy deposited measured by EC vs. track momentum $p_{\text{thres}}^{\text{high}}$ for positrons from π^0 events without the $g7$ lepton EC PID scheme applied. The red region depicts the cut that would reject events in the $g7$ lepton EC PID scheme.

4 Flux Determination

The photon flux is based on the flux procedure outline in Ref. [**clas.flux.note**]. The script to generate the photon flux for g12 is here:

```
/home/clasg12/local/scripts/g12-gflux
```

and there is also a script (/home/clasg12/local/scripts/g12-gflux-all) that doesn't rebin the energies and outputs two columns: energy and flux for each logical paddle in the tagger.

The help output from the script:

```
> /home/clasg12/local/scripts/g12-gflux -h
usage: g12-gflux emin emax ebinwidth runlist.txt (good|all)
      (good|all) specifies either all scalar intervals
      or only "good" scalar intervals.
example:
      g12-gflux 1.5 5.5 0.2 runlist.txt good
where runlist.txt is an ascii file of one column: run
56363
56365
...

```

To use the script, you will need to create a file that consists of the run numbers you used in your analysis. Using this filename when you call g12-gflux, will give you the total flux as a function of beam energy in the range and binning requested. The command:

```
/home/clasg12/local/scripts/g12-gflux 1.5 5.5 0.2 filelist.txt good
```

will return to stdout the flux in the energy bins using three columns: emin, emax, flux. Something like this:

```
1.5 1.7 7.75466725993e+12
1.7 1.9 7.23861294572e+12
1.9 2.1 6.85242336788e+12
... [snip] ...
4.9 5.1 2.69244768955e+12
5.1 5.3 2.49808049501e+12
5.3 5.5 1.99322166816e+12
```

The option good or all can be used to specify if you only want to consider good regions, throwing out beam trips, or if you want all events from good scalar intervals as well as the beam trip regions.

An alternative script which doesn't rebin the data but returns the flux for each logical energy paddle can be run like this:

```
/home/clasg12/local/scripts/g12-gflux-all filelist.txt good
```

The script has been extensively tested on the 64-bit machines. The precision of all variables are adequate to provide at least 4 significant figures for the final flux numbers.

The major caveat to using this script, which relies on gflux, is that you must included *whole runs* in your analysis for this to be accurate. This is because the gflux program was not designed to work with partial runs. So, you must verify that you have processed every file in the runs which were analyzed – one can use the g12runs program to aid in this.

4.1 Beam Trips

4.2 Normalized Yields for Different Beam Conditions

4.3 Run-by-run Stability and Systematic Uncertainty of Flux

5 Simulations

5.1 Generating Events for Digitization

One may use the program genr8 for generating t-channel phase space events. It is driven by an input key file which describes the exclusive reaction. Typical usage to generate 10k events from 4.4 to 5.45 GeV in beam energy using the input file “n_pi-pipi+.input+” looks like this:

```
genr8 -M10000 -B4.4,5.45 -o3pi.gamp < n_pi-pi+pi+.input
```

See the genr8 documentation for how to write the input file, or you can see this example here:

http://clasweb.jlab.org/rungroups/g12/wiki/index.php/N_pimpippip

Gsim requires a bos file with a PART bank containing the MC event. Note PART bank 0 is reserved for MC events whereas PART banks 1 and 2 are used for containing the reconstructed event. The best way to convert GAMP to PART banks is by using gamp2part – the command following the example above is:

```
gamp2part -r56855 -o3pi.part -T -S-0.321,0.378,-0.254,0.407 \
-z-110,-70 genr8.gamp
```

This writes a BOS file full of PART, sector 0 banks with the 4-vector information from the gamp file. Also, the -z option smears the target distribution in Z, while the -S smears it in X and Y. The parameters are means and sigmas of a 2D gaussian which were derived from a fit to the data. An alternative way to convert a gamp file to a BOS PART bank file is using gamp2txt and txt2part. These programs are piped together during run time.

```
gamp2txt -E5.714 -z-110,-70 < 3pi.gamp | txt2part -T -o3pi.part
```

The above command takes in gamp events, smears the z vertex in the target range, creates a tagger hit and writes out a bos file with HEAD, PART, and TAGR banks. Here is a bosdump of an event:

```
ifarml1> bosdump 3pi.part -M1
Group: HEAD Sector: 0 Nhits: 1 Next ind: 0
Version: 0
Run: 1
```

```

Event:          1
Type:          -2 (GSIM monte carlo)
ROC:           0
CLASS:         15
Trgbit:        0x1
TIME:          Wed Feb 27 22:16:00 2008

```

```

Group: PART    Sector: 0      Nhits: 3 Next ind: 0
pid: 8
  vert-> x: 0.000 y: 0.000 z: -95.178
  p-> E: 3.194 px: -0.591 py: -0.688 pz: 2.942
  q: 1.000 trkid: 0 qpid: 0.000 qtrk: 0 flags: 0
pid: 9
  vert-> x: 0.000 y: 0.000 z: -95.178
  p-> E: 3.194 px: -0.591 py: -0.688 pz: 2.942
  q: -1.000 trkid: 0 qpid: 0.000 qtrk: 0 flags: 0
pid: 8
  vert-> x: 0.000 y: 0.000 z: -95.178
  p-> E: 4.780 px: -0.246 py: -0.140 pz: 4.383
  q: 1.000 trkid: 0 qpid: 0.000 qtrk: 0 flags: 0

Group: TAGR    Sector: 0      Nhits: 1 Next ind: 0
ERG:5.001 TTAG:0.000 TPHO:0.000 STAT:15 T_id:17 E_id:82

```

One can use any alternative to genr8 as long as the output is either gamp or an appropriate BOS file. For example, there is the phase-space generator ppgen:

```

ppgen -M<reaction code> -P<photon energy> -E5.714 -j1 -G -A \
-t<t-slope> -m50000 > file.gamp

```

The output can be txt or gamp file depending on user's needs. Follow the previous instructions to convert to part banks as needed.

5.2 Digitization and Smearing

The program to track the particles through the simulation and ultimately digitize the information to simulated “raw” banks is the geant3-based program: gsim. Running this on the BOS file created above looks like this:

```
gsim_bat -ffread ffread.g12 -kine 1 -mcin 3pi.part -bosout 3pi.gsim -trig 2000000
```

Using the above command, should create a gsim bos outfile. Here is the FFREAD file should be used to run gsim_bat for g12 analyses:

```

====BEGIN=====FFREAD.G12=====
CUTS   5.e-3 5.e-3 5.e-3 5.e-3 5.e-3
DCCUTS 1.e-4 1.e-4 1.e-4 1.e-4 1.e-4

```

```
ECCUTS 1.e-4 1.e-4 1.e-4 1.e-4 1.e-4
SCCUTS 1.e-4 1.e-4 1.e-4 1.e-4 1.e-4
```

```
MAGTYPE 2
MAGSCALE 0.500 0.000
PTGIFIELD 0
STTYPE 1
STZOFF -90.0
TGPOS 0. 0. 0.
TARGET 'g11a'
TGMATE 'PROT'
POSBEAM 0.0 0.0
```

```
GEOM 'ALL' 'ST'
NOGEOM 'MINI' 'PTG '
BEAM 0 0 5.714
DCAY 1
KINE 1
MULS 1
AUTO 1
```

```
RUNG 56855
TIME 1000000 1000000 1000000
TRIG 1000000
STOP
====END=====FFREAD.G12=====
```

The tracking and digitization done by gsim is ideal and there is no smearing done. To get the simulated data to mimic the detector resolution the “gsim post-processor” (gpp) is used. For g12, and following the above example, one should use this command:

```
gpp -Y -s -S -a2.73 -b1.7 -c1.93.-f1 -R56855 -P0x7f -ogenr8.gpp genr8.gsim
```

The values passed to the gpp command line options, -a, -b, -c, helps match the tracking resolution of the simulated data to that of the real events in the regions 1,2 and 3 of the CLAS Drift Chambers. They accomplish this by smearing the DOCA values and hence gpp is able to match the DC residuals for the simulated CLAS tracks to that of the real CLAS tracks on a region-by-region basis. The gpp option -f smears the Time-of-Flight tdc values and during analysis the default gpp smearing for TOF was found to be adequate. The smearing should be run with a good g12 run number; run 56855 has all the necessary constants in the database to get the tagger timing smearing done correctly. Also, interested parties can add accidentals to the TAGR bank by using the -A option like so:

```
gpp -Y -s -S -a2.73 -b1.7 -c1.93 -f1 -R56855 -P0x7f -ogenr8.gpp \
-A/path/to/output/from/filter_tagr genr8.gsim
```

The program filter_tagr scans through real data files and outputs a bos file containing only the TAGR banks. These files are then supplied to gpp with the -A option, and gpp puts the contents of these banks as

Table 19: Measure of Track Reconstruction Efficiency for sets of gpp parameters

Events Generated	Events Accepted	Reconstruction Acceptance	gpp -a	Smearing -b	Factors -c	-f
90000	1217	1.352%	1	1	1	1
90000	1161	1.29%	2.73	1.7	1.93	1
90000	1053	1.17%	2.73	1.7	1.93	2

accidentals in the MC TAGR bank. Output from `filter_tagr` for run 56855 can be found at:

```
/home/clasg12/local/etc/clas6/gpp_tagger_profile.bos
```

As stated earlier, the goal of using GPP is to simulate the experimental conditions as close as possible. So we smear the values of the DOCA for the simulated tracks with a single gaussian whose width is equal to the events weighted sum of the widths of the two gaussians fitted to the data from the run 56855. This makes the residual for a superlayer in the simulated data approximately equal to the weighted residual from the real data. The default available options for GPP specifies only three parameters ‘-a, -b, -c’ for DC DOCA smearing, where each parameter is responsible for the smearing of two superlayers (in one Region) of all six sectors. Hence, we choose a set of parameters based on the following fits as seen in Figs. 47 and 48, which gives us the best match on average between the different superlayers in the six sectors (see Fig. 49).

The smearing parameter ‘-f’ for the Time of Flight timing resolution is one of the GPP parameters that is usually used to match the quality of data and simulation. Using the reference run 56855, we observe that the default GPP smearing is adequate (see Figure 50).

These smearing parameters affect the reconstruction efficiency for the tracks in CLAS during simulations. A rudimentary analysis quantifying the effect is presented in Table 19. As expected, as the Drift chamber response becomes more noisy due to smearing of DOCA (higher DC residuals), the reconstruction and tracking efficiency in CLAS goes down.

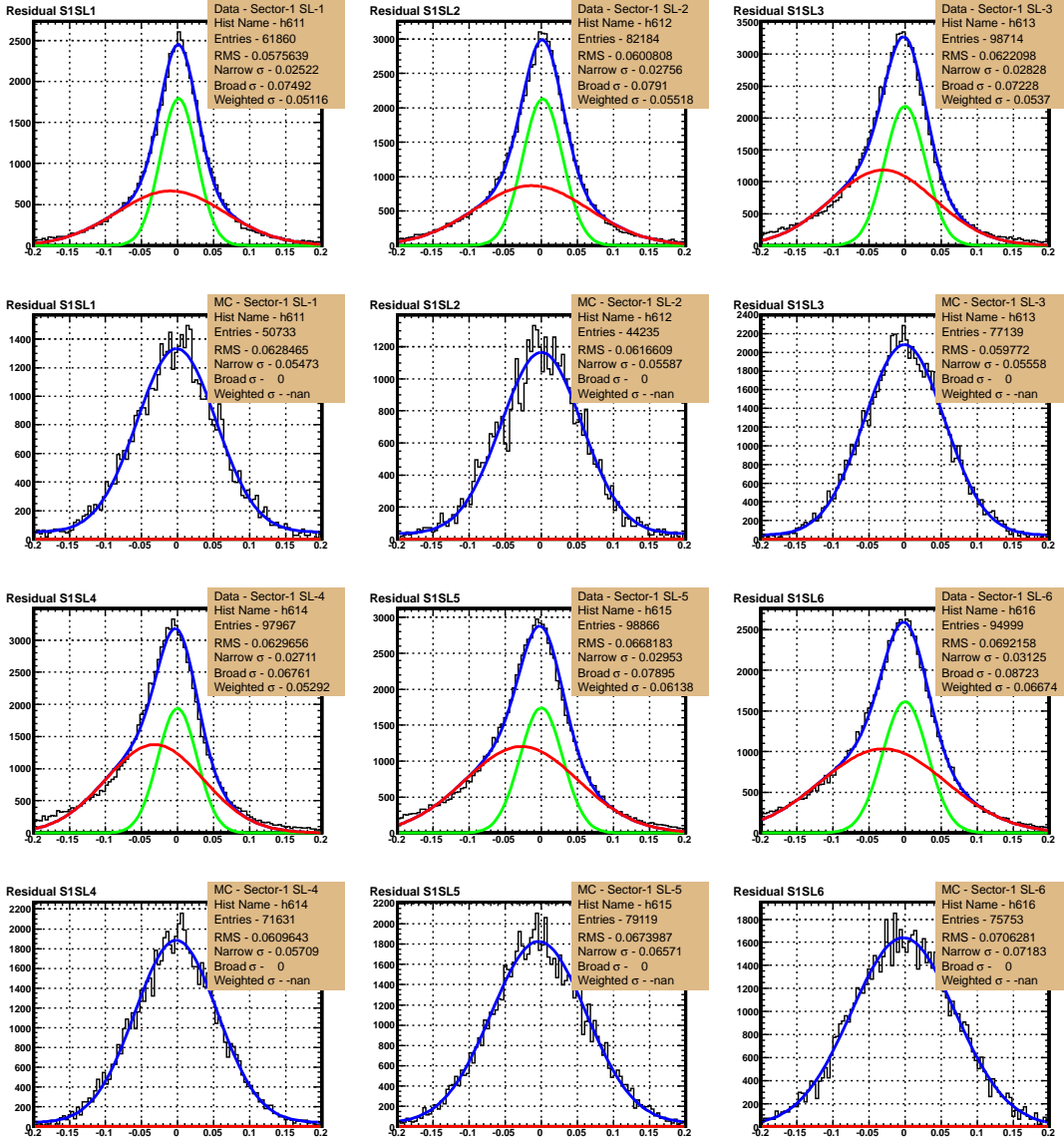


Figure 47: Plots and Fits used to match the residuals (resolution) for Drift Chamber superlayers in CLAS Sector 1, between the Data and the Simulation. Data is an empirical fit to a convolution of two gaussians. The simulated distribution is a single gaussian with its simulated width approximately equal to the weighed sum of the widths of the two gaussians fitted to the data. This simulation uses the best estimated smearing parameters to match the DC residuals, between the Data and the Simulation.

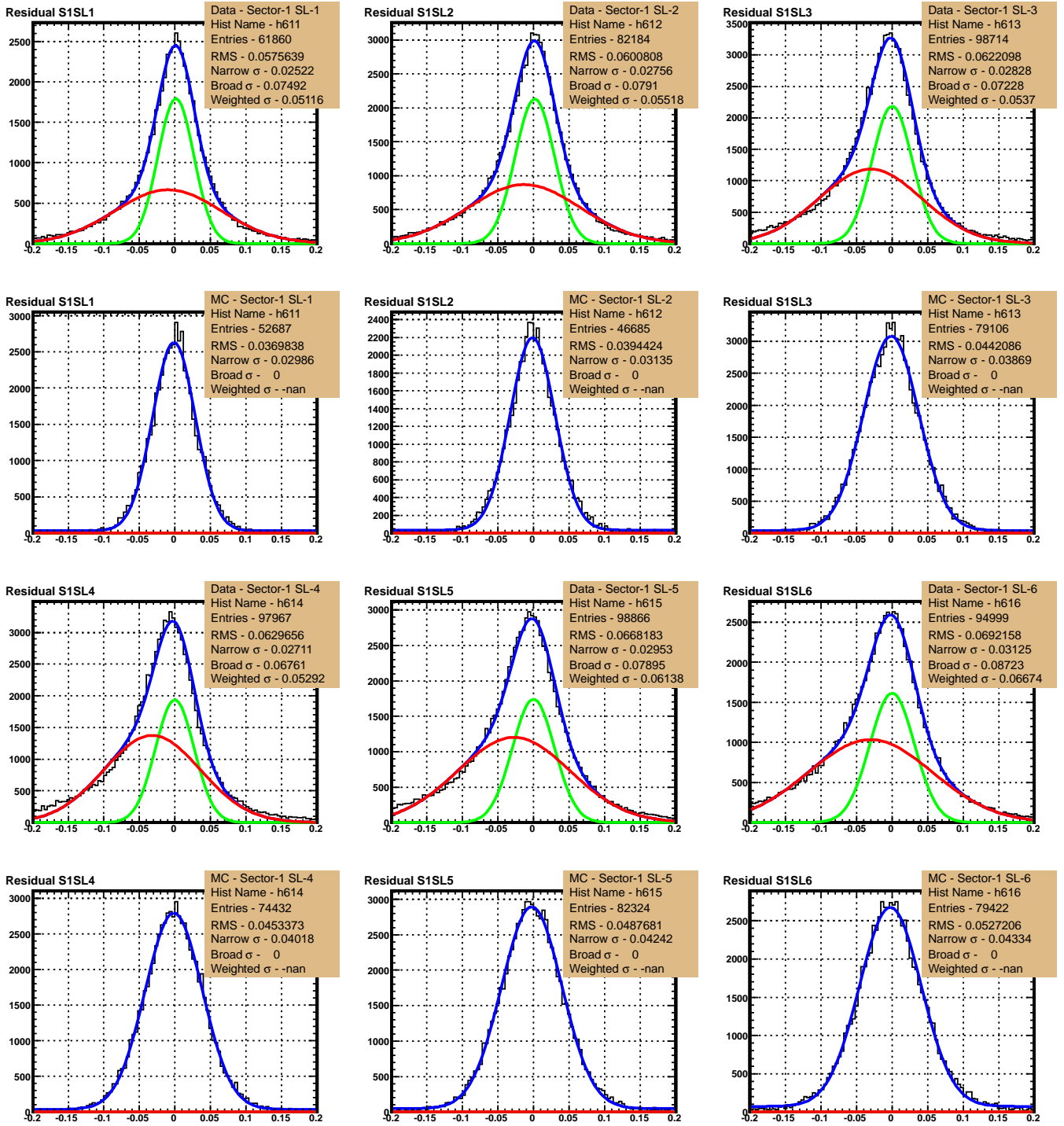


Figure 48: Plots and Fits used to compare the residuals (resolution) for Drift Chamber superlayers in CLAS Sector 1, between the Data and the Simulation using the default GPP smearing.

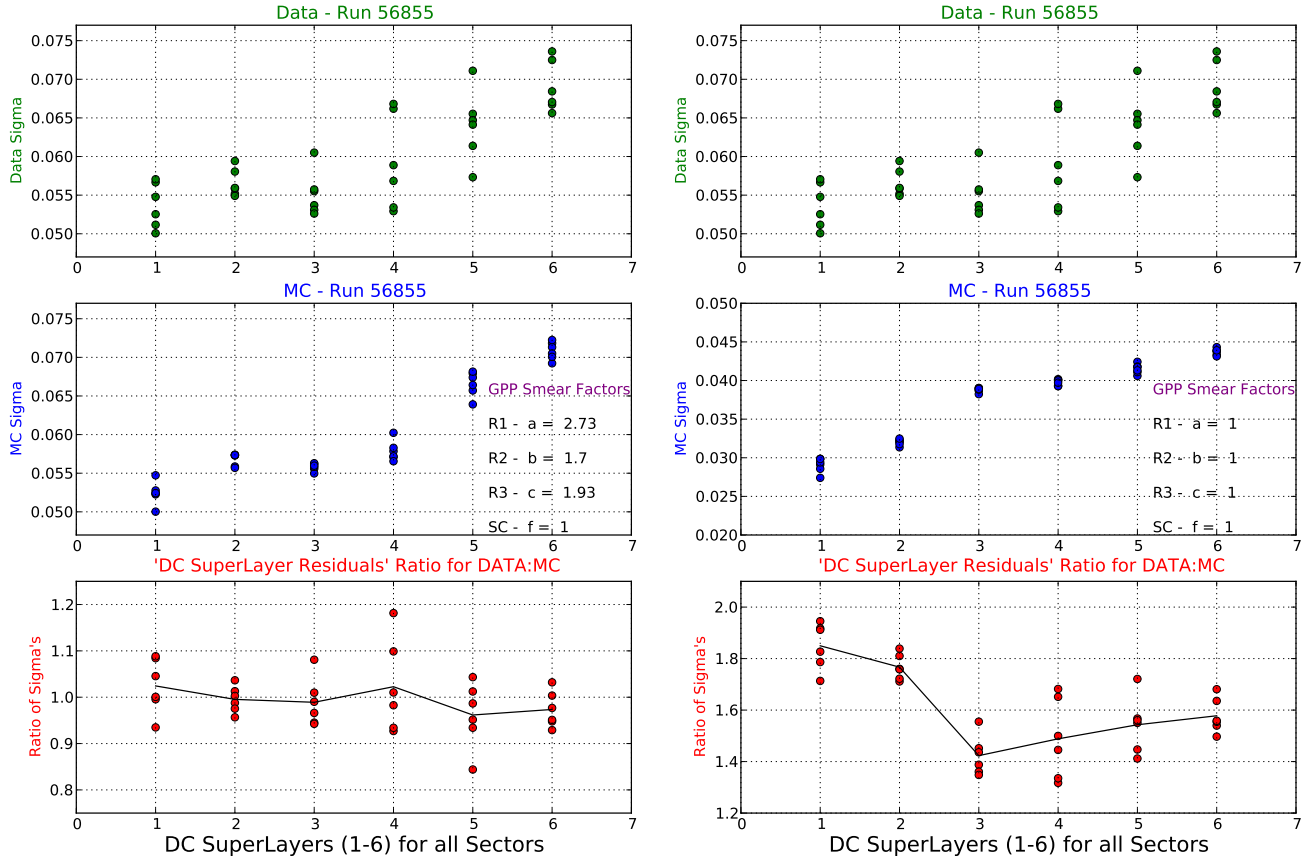


Figure 49: Comparison of the DC residuals on a superlayer basis for all the CLAS sectors for real as well as simulated events. The left plots use the best estimated smearing parameters for the DC DOCA to match the real and simulated data shown in Figure 47., whereas the right plots use the default GPP smearing shown in Figure 48.

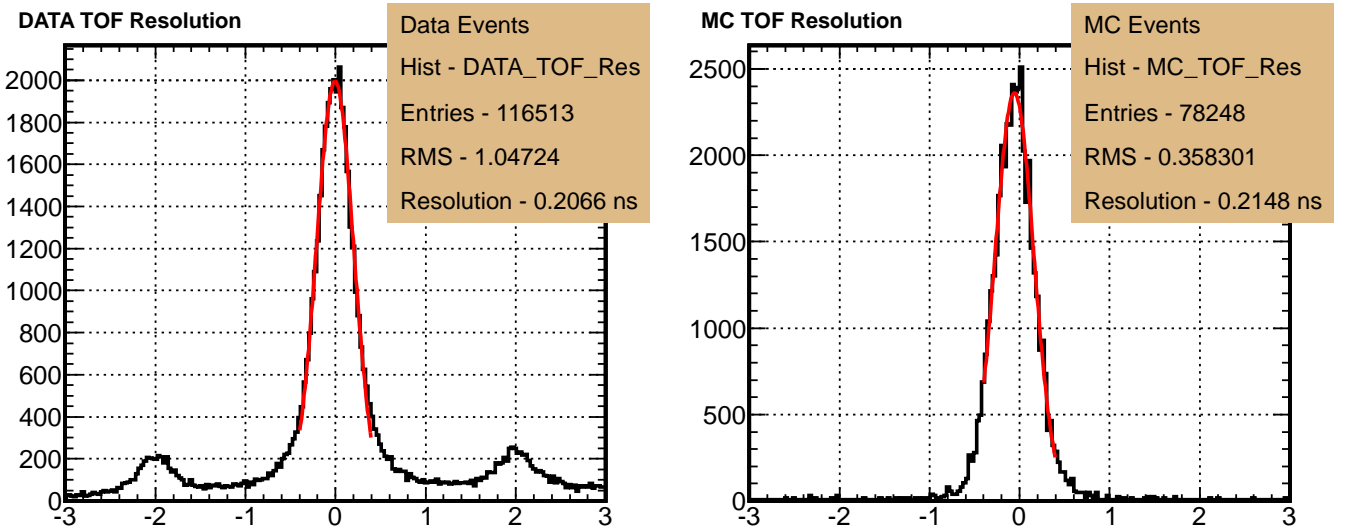


Figure 50: Plots and Fits used to match the TOF timing resolution. The default smearing of GPP was found to be adequate in this case.

5.3 Reconstruction of Simulated Data

5.4 Fiducial Region Selection

We derived *Geometric fiducial cuts* for the g12 data, which are cuts based on the exclusion of events laying outside regions where acceptance is well behaved and reliably reproduced in simulation. Such regions for all g12 data are expressed as an upper and lower limit of the difference in azimuthal angle between the center of a given sector, and a particle track. Because of the hyperbolic geometry of CLAS and the presence of the toroidal magnetic field, the fiducial boundaries on the angle ϕ are functions of momentum (p), charge, and polar angle (θ) of each track. The boundaries were evaluated separately in each sector, nominally defined as the ϕ values in which occupancy drops below 50% of that in the respective sector's flat region. The flat regions were defined as $-10^\circ < \phi < 10^\circ$. The nominal upper and lower ϕ limits depend strongly on particle charge, p and θ , hence the need for functional characterization and extrapolation.

In order to determine the fiducial limits for charged hadrons, a sample of exclusive $\gamma \pi \rightarrow p \pi^+ \pi^-$ events were sliced into $5 \times 15 \times 6$ bins in p , θ , and sector respectively. The ϕ distributions for π^+ and π^- were plotted separately in each bin. The upper and lower ϕ limits of these *first-generation* plots were found according to the nominal fiducial definition of 50% occupancy as illustrated in Fig. 51. The results from the first-generation fits were represented in *second-generation* plots of ϕ_{min} and ϕ_{max} vs θ as also shown in Fig. 51. The data in the second-generation plots were fit with hyperbolas, chosen since they replicate the projection of the detector. Second-generation fitting parameters were then plotted vs p in *third-generation* plots. These third generation plots were fit to power functions as shown in Fig. 52. Results of the third-generation fits define the sought after functional form $\phi_{min}(\theta, p)$ and $\phi_{max}(\theta, p)$ for each sector. The sector integrated results for positive and negative hadron tracks compose the nominal fiducial region. *Tight cuts* and *loose cuts* were defined as a contraction and expansion respectively, by 4° from the nominal fiducial cuts. Figs. 53-56 show the effects of the cuts.

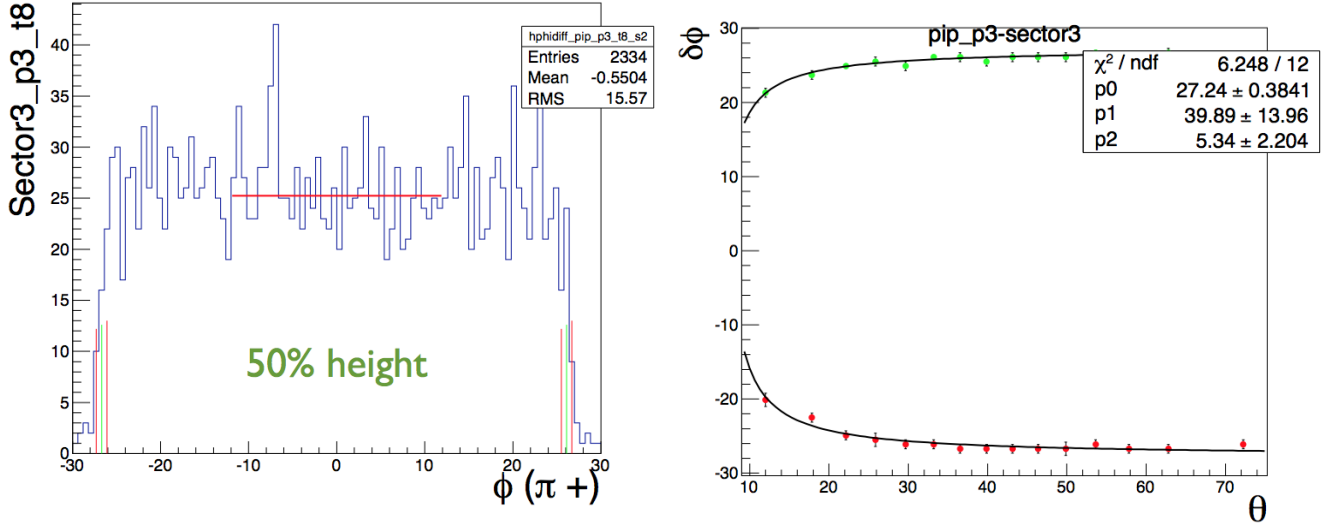


Figure 51: Left: shows the π^+ ϕ distribution for sector-three in one p and θ bin along with the upper and lower limits of the fiducial region represented by the green vertical line. Right: a second-generation plot, fit to a hyperbola.

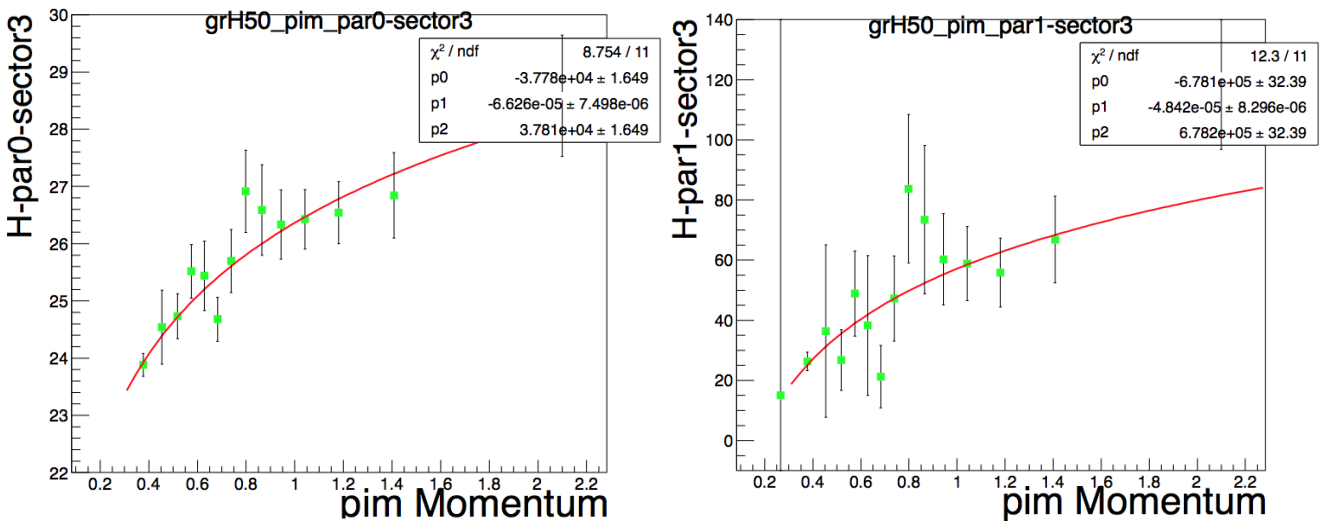


Figure 52: Third-generation plots of the fitting parameters from second-generation fits for sector three. The data are fit to power functions.

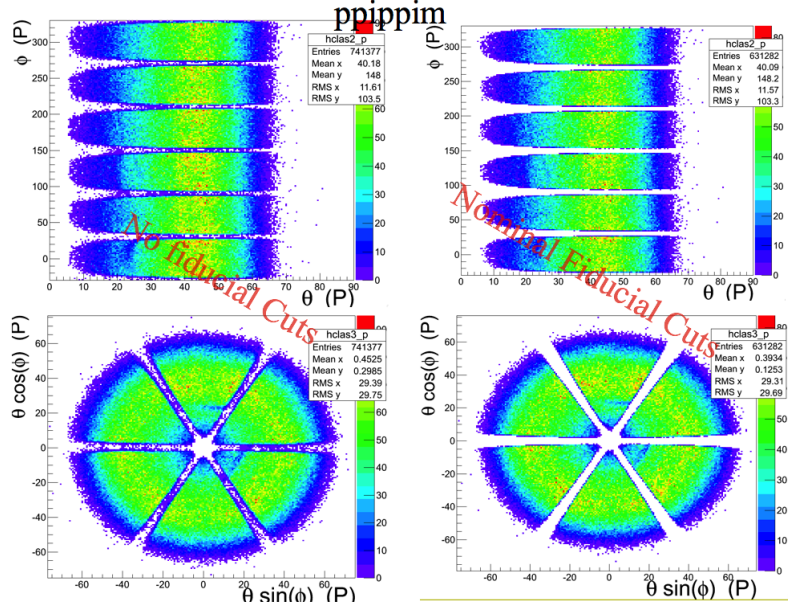


Figure 53: The angular distribution of the proton from exclusive $p\pi^+\pi^-$ events is shown. In the top, ϕ vs θ is plotted, the bottom plots conveys similar information mapped to mimic the geometry of CLAS. Left: No fiducial cuts. Right: nominal fiducial cuts on the proton.

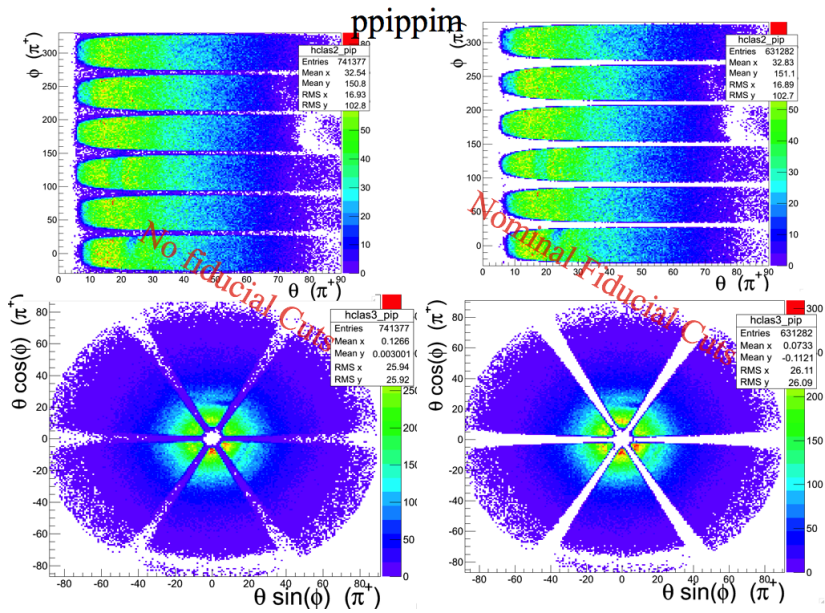


Figure 54: The angular distribution of the positive pion from exclusive $p\pi^+\pi^-$ events is shown. In the top, ϕ vs θ is plotted, the bottom plots conveys similar information mapped to reflect the geometry of CLAS. Left: no fiducial cuts. Right: nominal fiducial cuts on the positive pion.

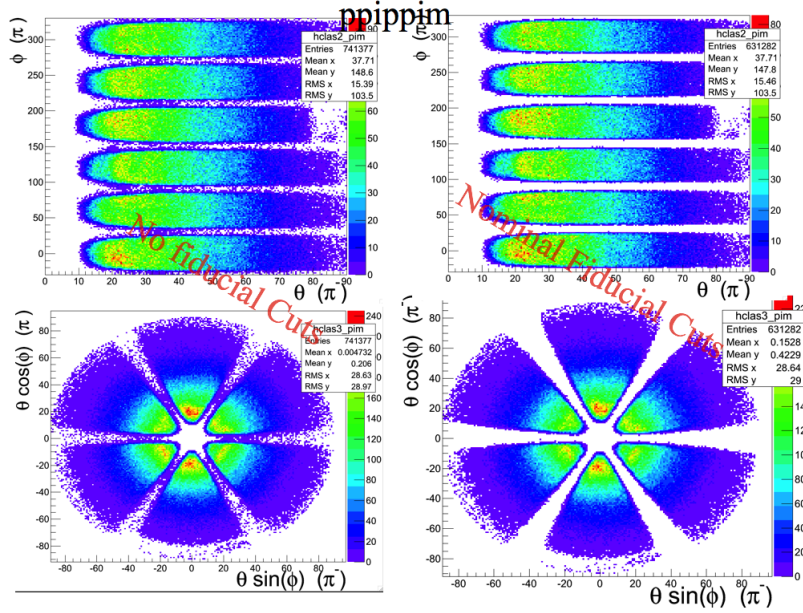


Figure 55: The angular distribution of the negative pion from exclusive $p\pi^+\pi^-$ events is shown. In the top, ϕ vs θ is plotted, the bottom plots conveys similar information mapped to reflect the geometry of CLAS. Left: no fiducial cuts. Right: nominal fiducial cuts on the negative pion.

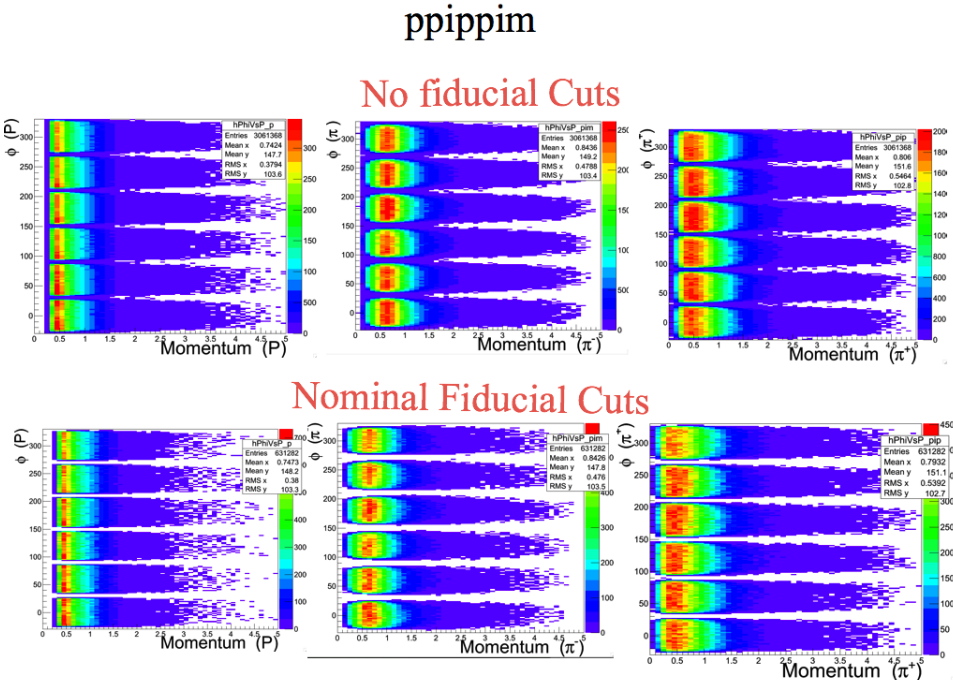


Figure 56: From left to right: ϕ vs momentum for the proton, negative pion and positive pion for $p\pi^+\pi^-$ events. Top: no fiducial cuts. Bottom: nominal fiducial cuts.

6 Other Systematics

6.1 Comparison of Data to Known Resonances

6.2 Comparison of Data to Known Cross Sections

References

- [1] John T. Goetz. “ Ξ Hyperon Photoproduction from Threshold to 5.4 GeV with the CEBAF Large Acceptance Spectrometer”. PhD thesis. University of California Los Angeles, 2010.
- [2] Craig Bookwalter. “A Search for Exotic Mesons in $\gamma p \rightarrow \pi^+ \pi^+ \pi^- n$ with CLAS at Jefferson Lab”. PhD thesis. Florida State University, 2012.
- [3] Diane Schott. “A Search for an Exotic Meson in the $\gamma p \rightarrow \Delta^{++} \pi^- \eta$ Reaction”. PhD thesis. Florida International University, 2012.
- [4] Mukesh Saini. “Search for New and Unusual Stangonia using CLAS”. PhD thesis. Florida State University, 2013.
- [5] Jason Bono. “First Time Measurements of Polarization Observables for the Charged Cascade Hyperon in Photoproduction”. PhD thesis. Florida International University, 2014.